NASA Technical Memorandum 110347

Aerodynamics Model for a Generic ASTOVL Lift-Fan Aircraft

Lourdes G. Birckelbaw, Walter E. McNeill, and Douglas A. Wardwell, Ames Research Center, Moffett Field, California

April 1995

National Aeronautics and
Space Administration

Ames Research Center
Moffett Field, California 94035-1000

Nomenclature

A_j	individual jet exit area, ft^2
$A_{J,total}$	total jet exit area, ft^2
b	wing span, ft
$\bar{c}$	mean aerodynamic chord, ft
C_D	drag coefficient
CGFS	fuselage station center of gravity, in.
CGWL	waterline center of gravity, in.
C_l	rolling moment (RM) coefficient
C_{l_β}	rolling moment due to sideslip derivative, 1/rad
C_{l_p}	rolling moment due to roll rate derivative, 1/rad
C_{l_r}	rolling moment due to yaw rate derivative, 1/rad
$C_{l_{\delta rud}}$	rolling moment due to rudder deflection derivative, 1/rad
C_L	lift coefficient
C_{L_q}	lift coefficient due to pitch rate derivative, 1/rad
$C_{L_{\dot{\alpha}}}$	lift coefficient due to angle-of-attack rate derivative, 1/rad
C_m	pitching moment (PM) coefficient
C_{m_q}	pitching moment due to pitch rate derivative, 1/rad
$C_{m_{\dot{\alpha}}}$	pitching moment due to angle-of-attack rate derivative, 1/rad
C_n	yawing moment (YM) coefficient
C_{n_β}	yawing moment due to sideslip derivative, 1/rad
C_{n_p}	yawing moment due to roll rate derivative, 1/rad
C_{n_r}	yawing moment due to yaw rate derivative, 1/rad
$C_{n_{\delta rud}}$	yawing moment due to rudder deflection derivative, 1/rad
C_y	side force (FY) coefficient
C_{y_β}	side force due to sideslip derivative, 1/rad
C_{y_p}	side force due to roll rate derivative, 1/rad
$C_{y_{\delta rud}}$	side force due to rudder deflection derivative, 1/rad
d_e	total equivalent circular jet diameter, ft: $d_e = 2\sqrt{A_{j,total}/\pi}$
D	drag, lb
FY	side force, lb
GE	ground effect
h	aircraft height from the bottom of the fuselage, ft
h/d_e	nondimensional aircraft height
IGE	in-ground effect
K_{GE}	ground effect washout factor
L	lift, lb
LF	lift fan
LN	lift nozzle
MRC	moment reference center
PM	pitching moment, ft-lb
q	pitch rate, rad/sec
$\bar{q}$	dynamic pressure, lb/ft^2
RM	rolling moment, ft-lb
RN	rear nozzle, same as lift nozzle
S	wing area, ft^2
T	total thrust, lb: $T = T_{LF} + T_{LN}$
T_{LF}	thrust of the lift fan, lb
T_{LN}	thrust of the lift nozzles, lb
V_e	equivalent jet velocity ratio: $V_{e,j} = \sqrt{q_\infty / q_j} = \sqrt{2A_j q_\infty / T_j}$
X_{MRC}	X-axis moment arm for varying CGFS, in.
YM	yawing moment, ft-lb
Z_{MRC}	Z-axis moment arm for varying CGWL, in.
α	angle of attack, deg
β	sideslip angle, rad

δail	aileron deflection angle, deg
δcanard	canard deflection angle, deg
δflap	flap deflection angle, deg
δrud	rudder deflection angle, rad
δ_{EQ}	equivalent jet angle, deg: $\delta_{EQ} = \lambda(\delta_{LF}) + (1 - \lambda)\delta_{LN}$
δ_{LF}	lift-fan nozzle deflection angle, deg
δ_{LN}	lift nozzle deflection angle, deg
$\Delta C_{D_{IGE}}$	unpowered in-ground effect drag increment
$\Delta C_{L_{IGE}}$	unpowered in-ground effect lift increment
$\Delta C_{m_{IGE}}$	unpowered in-ground effect pitching moment increment
$\Delta L/T$	nondimensionalized jet-induced lift increment
λ	thrust split: $\lambda = T_{LF}/T$

Aerodynamics Model for a Generic ASTOVL Lift-Fan Aircraft

LOURDES G. BIRCKELBAW, WALTER E. MCNEILL, AND DOUGLAS A. WARDWELL

Ames Research Center

Summary

This report describes the aerodynamics model used in a simulation model of an advanced short takeoff and vertical landing lift-fan fighter aircraft. The simulation model was developed for use in piloted evaluations of transition and hover flight regimes, so that only low speed (M ~ 0.2) aerodynamics are included in the mathematical model. The aerodynamics model includes both the power-off aerodynamic forces and moments and the propulsion system induced aerodynamic effects.

Introduction

NASA Ames Research Center is participating in technology development for advanced short takeoff and vertical landing (ASTOVL) fighter aircraft as a member of the Joint Advanced Strike Technology (JAST) and formerly the Advanced Research Projects Agency (ARPA) ASTOVL program. Integration of flight and propulsion controls is one of the critical technologies being pursued in that program. NASA's role in this technical area is to participate in developing design guidelines for integrated flight/propulsion controls, support technology development for ASTOVL demonstrator aircraft, and provide consultation on integrated control design to the program contractors. Specifically, NASA will carry out design guideline analyses for the control system and conduct piloted simulations on the Ames Research Center Vertical Motion Simulator (VMS) to evaluate design guidelines and to assess the merits of contending design approaches.

The initial effort in this program was to develop a mathematical model for simulation of a representative ASTOVL aircraft concept. This simulation model was used in an experiment on the VMS to gain initial experience with control system behavior and flying qualities for this aircraft concept. A description of the representative ASTOVL aircraft's integrated flight/propulsion control system, head-up display and the propulsion system performance and dynamic response is provided in reference 1. This report describes the representative aircraft's subsonic, power-off aerodynamics and jet-induced aerodynamics in hover and forward flight, including ground effects.

Description of the ASTOVL Lift-Fan Aircraft

The representative ASTOVL lift-fan aircraft is a single-place, single-engine fighter/attack aircraft, featuring a wing-canard arrangement with twin vertical tails, as shown in figure 1. Geometric characteristics of the configuration are summarized in table 1; mass properties are specified in table 2.

The propulsion system concept is presented in figure 2. It consists of a remote lift fan coupled to a lift cruise turbofan engine to permit continuous transfer of energy from the lift cruise engine to the lift fan. The lift cruise engine exhaust is either ducted aft to a thrust deflecting cruise nozzle in conventional flight, or diverted to two deflecting lift nozzles in vertical flight. Throughout transition flow can be continuously transferred between the cruise and lift nozzles. Lift-fan and lift-nozzle thrust can be deflected from 45 to 100 deg below the aircraft waterline. The cruise nozzle can be deflected ±20 deg vertically.

The basic flight control system consists of the canard, ailerons, and twin rudders for aerodynamic effectors during forward flight. For powered-lift operation, control is provided by differential thrust transfer between the lift fan and lift nozzles, deflection of lift-fan and lift-nozzle thrust, and deflection of cruise-nozzle thrust. Pitch control is achieved by a combination of canard deflection, thrust transfer between the lift fan and lift nozzles, and deflection of the cruise nozzle. Roll control is produced by the ailerons and differential thrust transfer between the lift nozzles. Yaw control is derived from the combination of rudder deflection, differential lift-nozzle deflection, and lateral lift-fan thrust deflection. As an option, reaction control, powered by the engine compressor bleed air, can provide additional control moments through nozzles located in the wing extremities and in the tail. Longitudinal acceleration is achieved through thrust transfer between the lift fan, lift nozzles, and cruise nozzles and by deflection of the lift-fan and lift-nozzle thrust.

Aerodynamics Model

The aerodynamics model includes both the power-off aerodynamic forces and moments and the propulsion system induced aerodynamic effects. The simulation experiment focused on transition and hover flight regimes, so that only low-speed (M ~ 0.2) aerodynamics are included in the mathematical model.

The power-off aerodynamics data were generated using the U.S. Air Force Stability and Control Digital DATCOM program (ref. 2) and a NASA Ames in-house graphics program called VORVIEW (no reference available) which allows the user to easily analyze arbitrary conceptual aircraft configurations using the VORLAX program (which is based on the vortex lattice method of ref. 3). All the power-off coefficients and derivatives were calculated in the stability axes. The jet-induced data were generated using the prediction methods of references 4–8. For the data shown in this report, the moment reference for Digital DATCOM was 30.889 ft aft of the nose, the moment reference for VORVIEW/ VORLAX was 31.204 ft aft of the nose (–10 percent of the mean aerodynamic chord), and the moment reference for the jet-induced effects was 31.11 ft aft of the nose. In the final simulation model, these data were all transferred to a moment reference center of 31.11 ft.

Due to certain Digital DATCOM limitations, some derivatives required special treatment because of the canard configuration. For the $\dot{\alpha}$ derivatives, $C_{L_{\dot{\alpha}}}$ and $C_{m_{\dot{\alpha}}}$, DATCOM methods do not exist for a ratio of forward-surface span to aft-surface span less than 1.5. To satisfy this requirement, the aft surface was truncated to a span just less than two-thirds that of the canard. This was considered a better choice than assuming the derivatives were zero.

Also, the digital DATCOM program had no provision for directly calculating the effects of deflected rudders. The rudder effectiveness derivatives, $C_{y_{\delta rud}}$, $C_{l_{\delta rud}}$, and $C_{n_{\delta rud}}$, were calculated by replacing the wing and canard with an aft horizontal surface with exposed geometry identical to that of the vertical tails and attached to a radically slimmed body. At zero angle of attack, the trailing-edge surfaces were deflected differentially, as ailerons would be, and the change in rolling moment coefficient was calculated. The same surfaces were deflected symmetrically to generate changes in the lift coefficient and the pitching moment coefficient, which were converted to side force and yawing moment coefficients, respectively. All coefficients were calculated using the normal wing (aft lifting surface) reference geometry.

The unpowered in-ground effects, $\Delta C_{L_{IGE}}$, $\Delta C_{D_{IGE}}$, and $\Delta C_{m_{IGE}}$, were calculated by Digital DATCOM as functions of angle of attack for a height of 6 ft at the wing 25 percent mean aerodynamic chord. For this purpose, the configuration consisted of only the wing and regular (unslimmed) body.

The longitudinal aerodynamics terms are discussed next and are followed by the lateral directional terms.

Longitudinal Aerodynamics

Lift– The lift equation for the lift-fan model is shown in equation 1. The first term in this equation represents the power-off lift, and the second term represents the lift increment due to jet-induced effects.

$$L = C_L \bar{q} S + \frac{\Delta L}{T} T \tag{1}$$

The equation for C_L is shown in equation 2. Lift curves for $C_L(\alpha, \delta\text{flap})$ and $C_L(\alpha, \delta\text{canard})$ are shown in figures 3 and 4, respectively. The curves shown in figures 3 and 4 were generated using the vortex-lattice program previously mentioned. Digital DATCOM was used to predict the pitch rate derivative, $C_{L_q} = 0.746/\text{rad}$, and the $C_{L_{\dot{\alpha}}}(\alpha)$ curve, shown in figure 5. Digital DATCOM was also used to predict the lift coefficient increment due to the influence of the ground plane, $\Delta C_{L_{IGE}}(\alpha)$, shown in figure 6, as well as the ground effect washout factor, K_{GE}, shown in figure 7.

$$C_L = C_L(\alpha, \delta\text{flap}) + \Delta C_{L_{\delta\text{canard}}} + C_{L_q} \frac{q\bar{c}}{2U_B} + C_{L_{\dot{\alpha}}}(\alpha) \frac{\dot{\alpha}\bar{c}}{2U_B} + K_{GE} \Delta C_{L_{IGE}}(\alpha) \tag{2}$$

where

$$\Delta C_{L_{\delta\text{canard}}} = C_L(\alpha, \delta\text{canard}) - C_L(\alpha, \delta\text{canard} = 0°) \tag{2a}$$

The expression for the jet-induced lift increment, $\Delta L/T$, is presented in equation 3. Note that the lift fan and lift nozzle terms use their respective nozzle angles, δ, and velocity ratios, V_e. However, the fountain term uses the aircraft's equivalent nozzle angle and velocity ratio.

$$\frac{\Delta L}{T} = \left[\frac{\Delta L}{T}\left(\frac{h}{d_e}, \delta_{LF}, V_{e,LF}\right)\right]_{LF} + \left[\frac{\Delta L}{T}\left(\frac{h}{d_e}, \delta_{LN}, V_{e,LN}\right)\right]_{LN} + \left[\frac{\Delta L}{T}\left(\frac{h}{d_e}, \delta_{EQ}, V_{EQ}\right)\right]_{Fount} \quad (3)$$

Figures 8–11 show the jet-induced lift increment due to the lift fan for nozzle angles of 90, 75, 60, and 45 deg, respectively. Figures 12–15 show the jet-induced lift increment due to the lift nozzles for angles of 90, 75, 60, and 45 deg, respectively. Figures 16–19 show the jet-induced lift increment due to the fountain for equivalent (lift fan and lift nozzle, δ_{EQ}) angles of 90, 75, 60, and 45 deg, respectively.

Drag– The drag equation for the lift-fan model is shown in equation 4. This equation accounts only for the power-off drag.

$$D = C_D \bar{q} S \quad (4)$$

The equation for C_D is shown in equation 5. Drag curves for $C_D(\alpha, \delta flap)$ and $C_D(\alpha, \delta canard)$ are shown in figures 20 and 21, respectively. The curves shown in figures 20 and 21 were generated using the vortex-lattice program. Digital DATCOM was used to predict the drag coefficient increment due to the influence of the ground plane, $\Delta C_{D_{IGE}}(\alpha)$, shown in figure 22.

$$C_D = C_D(\alpha, \delta flap) + \Delta C_{D_{\delta canard}} + K_{GE}\Delta C_{D_{IGE}}(\alpha) \quad (5)$$

where

$$\Delta C_{D_{\delta canard}} = C_D(\alpha, \delta canard) - C_D(\alpha, \delta canard = 0°) \quad (5a)$$

Pitching moment– The pitching moment equation for the lift-fan model is shown in equation 6. The first term in the equation represents the power-off pitching moment, the second term represents the jet-induced pitching moment increment, and the remaining terms account for center-of-gravity (c.g.) travel.

$$PM = C_m \bar{q} S \bar{c} + \frac{\Delta PM}{Td_e} Td_e + (L\cos\alpha + D\sin\alpha)X_{MRC} + (L\sin\alpha - D\cos\alpha)Z_{MRC} \quad (6)$$

The equation for C_m is shown in equation 7. Pitching moment curves for $C_m(\alpha, \delta flap)$ and $C_m(\alpha, \delta canard)$ are shown in figures 23 and 24, respectively. The curves of figure 23 were generated using the vortex-lattice program. The curves shown in figure 24 were generated using Digital DATCOM. DATCOM was also used to predict the pitch rate derivative, $C_{m_q} = -1.589$/rad, the curve for $C_{m_{\dot\alpha}}(\alpha)$, shown in figure 25, and the pitching moment coefficient increment due to the influence of the ground plane, $\Delta C_{m_{IGE}}(\alpha)$, shown in figure 26.

$$C_m = C_m(\alpha, \delta flap) + \Delta C_{m_{\delta canard}} + C_{m_q}\frac{q\bar{c}}{2U_B} + C_{m_{\dot\alpha}}(\alpha)\frac{\dot\alpha\bar{c}}{2U_B} + K_{GE}\Delta C_{m_{IGE}}(\alpha) \quad (7)$$

where

$$\Delta C_{m_{\delta canard}} = C_m(\alpha, \delta canard) - C_m(\alpha, \delta canard = 0°) \quad (7a)$$

The expression for the jet-induced pitching moment increment, $\Delta PM/Td_e$, is presented in equation 8.

$$\frac{\Delta PM}{Td_e} = \left[\frac{\Delta PM}{Td_e}\left(\frac{h}{d_e}, \delta_{LF}, V_{e,LF}\right)\right]_{LF} + \left[\frac{\Delta PM}{Td_e}\left(\frac{h}{d_e}, \delta_{LN}, V_{e,LN}\right)\right]_{LN} + \left[\frac{\Delta PM}{Td_e}\left(\frac{h}{d_e}, \delta_{EQ}, V_{EQ}\right)\right]_{Fount} \quad (8)$$

Figures 27–30 show the jet-induced pitching moment increment due to the lift fan for nozzle angles of 90, 75, 60, and 45 deg, respectively. Figures 31–34 show the jet-induced pitching moment increment due to the lift nozzles for angles of 90, 75, 60, and 45 deg, respectively. Figures 35–38 show the jet-induced pitching moment increment due to the fountain for equivalent (lift fan and lift nozzle, δ_{EQ}) angles of 90, 75, 60, and 45 deg, respectively.

Lateral Directional Aerodynamics

The Digital DATCOM program was used to predict most of the lateral directional stability derivatives. The static derivatives, C_{y_β}, C_{l_β}, C_{n_β}, were obtained for the complete aircraft configuration by adding the individual airframe components: body, wing, canard, and vertical tails, a procedure which assumed the absence of interference.

Side force– The side force equation is shown in equation 9, and the expansion of the power-off side force coefficient is presented in equation 10.

$$FY = C_y \bar{q} S \tag{9}$$

$$C_y = C_{y_\beta}(\alpha)\beta + C_{y_p}(\alpha)\frac{pb}{2U_B} + C_{y_{\delta rud}}\delta rud + C_y(\alpha, \delta ail) \tag{10}$$

Digital DATCOM was used to predict the side force coefficients for $C_{y_\beta}(\alpha)$ and $C_{y_p}(\alpha)$; these curves are shown in figures 39 and 40, respectively. Digital DATCOM was used to predict the rudder derivative: $C_{y_{\delta rud}} = 0.2063$/rad. The side force coefficient due to aileron deflection, $C_y(\alpha, \delta ail)$, is shown in figure 41 and was generated using the vortex-lattice program.

Rolling moment– The rolling moment equation is shown in equation 11. The first term accounts for the power-off rolling moment, the second term represents the jet-induced rolling moment increment, and the third term accounts for c.g. travel.

$$RM = C_l \bar{q} S b + \frac{\Delta RM}{Td_e} Td_e + FY\, Z_{MRC} \tag{11}$$

The equation for C_l is presented in equation 12. Digital DATCOM was used to predict the rolling moment coefficients for $C_{l_\beta}(\alpha)$, $C_{l_p}(\alpha)$, $C_{l_r}(\alpha)$, and $C_{l_{\delta rud}}(\alpha)$; these curves are shown in figures 42–45, respectively. The rolling moment coefficient due to aileron deflection, $C_l(\alpha, \delta ail)$, is shown in figure 46 and was generated using the vortex-lattice program.

$$C_l = C_{l_\beta}(\alpha)\beta + C_{l_p}(\alpha)\frac{pb}{2U_B} + C_{l_r}(\alpha)\frac{rb}{2U_B} + C_{l_{\delta rud}}(\alpha)\delta rud + C_l(\alpha, \delta ail) \tag{12}$$

The jet-induced rolling moment increment, $\Delta RM/Td_e$, was predicted using the methods of reference 5, and is presented in equation 13. The prediction for rolling moment assumes that the effects of β are linear and should therefore be limited to $\beta < 10$ deg. Predictions for jet-induced rolling moment per degrees of sideslip in-ground effect could not be predicted; however, out-of-ground effect numbers were better defined. Therefore, only out-of-ground effect rolling moments due to sideslip were calculated and were assumed height independent.

$$\frac{\Delta RM}{Td_e} = \left[\frac{\Delta RM}{Td_e\beta}\left(\frac{h}{d_e}, \delta_{LF}, V_{e,LF}\right)\beta\right]_{LF} + \left[\frac{\Delta RM}{Td_e}\left(\frac{h}{d_e}, \delta_{LN}, V_{e,LN}\right)\beta\right]_{LN} + \left[\frac{\Delta RM}{Td_e}\left(\frac{h}{d_e}, \delta_{EQ}, V_{EQ}\right)\beta\right]_{Fount} \tag{13}$$

Figures 47–50 show the jet-induced rolling moment increment due to the lift fan for nozzle angles of 90, 75, 60, and 45 deg, respectively. Figures 51–54 show the jet-induced rolling moment increment due to the lift nozzles for angles of 90, 75, 60, and 45 deg, respectively. Since only out-of-ground effects were accounted for, and since the fountain is only felt in-ground effect, the fountain contribution was zero.

Yawing moment– The yawing moment equation is shown in equation 14. The first term accounts for the power-off yawing moment and the second term accounts for c.g. travel. The jet-induced yawing moment increment could not be predicted very well, but it was assumed to be small, and therefore neglected.

$$YM = C_n \bar{q} S b + FY\, X_{MRC} \tag{14}$$

The equation for C_n is presented in equation 15. Digital DATCOM was used to predict the yawing moment coefficients for $C_{n_\beta}(\alpha)$, $C_{n_p}(\alpha)$, $C_{n_r}(\alpha)$, and $C_{n_{\delta rud}}(\alpha)$; these curves are shown in figures 55–58, respectively. The yawing moment coefficient due to aileron deflection, $C_n(\alpha, \delta ail)$, is shown in figure 59 and was generated using the vortex-lattice program.

$$C_n = C_{n_\beta}(\alpha)\beta + C_{n_p}(\alpha)\frac{pb}{2U_B} + C_{n_r}(\alpha)\frac{rb}{2U_B} + C_{n_{\delta rud}}(\alpha)\delta rud + C_n(\alpha, \delta ail) \tag{15}$$

Conclusions

This report describes the aerodynamics model used in a simulation model of an advanced short takeoff and vertical landing lift-fan fighter aircraft. The simulation model was developed for use in piloted evaluations of transition and hover flight regimes, so that only low speed ($M \sim 0.2$) aerodynamics are included in the mathematical model. The aerodynamics model includes the power-off aerodynamic forces and moments and the propulsion system induced aerodynamic effects, including ground effects.

The power-off aerodynamics data were generated using the U.S. Air Force Stability and Control Digital DATCOM program and a NASA Ames in-house graphics program called VORVIEW which allows the user to easily analyze arbitrary conceptual aircraft configurations using the VORLAX program. The jet-induced data were generated using the prediction methods of R. E. Kuhn et al., as referenced in this report.

References

1. Chung, W. W. Y.; Borchers, P. F.; and Franklin, J. A.: Simulation Model of the Integrated Flight/Propulsion Control System, Displays, and Propulsion System for an ASTOVL Lift Fan Aircraft. NASA TM-108866, Apr. 1995.

2. Williams, J. E.; and Vukelich, S. R.: The USAF Stability and Control Digital DATCOM; Volumes I, II, and III. AFFDL-TR-79-3032, Apr. 1979.

3. Miranda, L. R.; Elliot, R. D.; and Baker, W. M.: A Generalized Vortex Lattice Method for Subsonic and Supersonic Flow Applications. NASA CR-2865, Dec. 1977.

4. Kuhn, R. E.; Stewart, V. R.; and Wardwell, D. A.: Estimation of Lift and Pitching Moment Induced on Jet STOVL Aircraft Hovering In Ground Effect. WL-TR-93-3046, Flight Dynamics Directorate, Wright Patterson Air Force Base, Ohio, Aug. 1993.

5. Kuhn, R. E.: An Engineering Method for Estimating the Lateral/Directional Characteristics of V/STOL Configurations in Transition. NADC 81031-60, Naval Air Development Center, Warminster, Pa., Feb. 1981.

6. Stewart, V. R.; and Kuhn, R. E.: A Method for Prediction of the Aerodynamic Stability and Control Parameters of STOL Aircraft Configurations; Volume II: STOL Aerodynamic Stability and Control Estimation Methods. AFWAL-TR-87-3019, vol. II, secs. 4 and 14, Flight Dynamics Laboratory, Wright Patterson Air Force Base, Ohio, June 1987.

7. Stewart, V. R.; and Kuhn, R. E.: A Method for Prediction of the Aerodynamic Stability and Control Parameters of STOL Aircraft Configurations; Volume III: General Backup Information, Derivation, and Verification. AFWAL-TR-87-3019, vol. III, secs. E, H, and K, Flight Dynamics Laboratory, Wright Patterson Air Force Base, Ohio, June 1987.

8. Henderson, C.; Clark, J.; and Walters, M.: V/STOL Aerodynamics, Stability & Control Manual (Supplement 1). NADC 80017-60, NAVAL Air Systems Command, Department of the Navy, Washington, D.C., Jan. 1983.

Table 1. Aircraft geometry

	Overall length	55.4 ft
	Overall height	14.16 ft
Wing	Area	523.3 ft^2
	Span	36.17 ft
	Mean aerodynamic chord	18.42 ft
	Aspect ratio	2.50
	Leading-edge sweep	40.0 deg
	Trailing-edge sweep	30.0 deg
	Airfoil	NACA 64A005
Canard	Area	243.1 ft^2
	Span	24.65 ft
	Mean aerodynamic chord	12.55 ft
	Aspect ratio	2.50
	Leading-edge sweep	40.0 deg
	Trailing-edge sweep	30.0 deg
	Airfoil	NACA 64A004.5
Vertical tail (each)	Area	39.0 ft^2
	Span	6.98 ft
	Mean aerodynamic chord	7.11 ft
	Aspect ratio	1.25
	Leading-edge sweep	40.0 deg
	Trailing-edge sweep	30.0 deg
	Airfoil	NACA 64A004.5

Table 2. Mass properties

Weight	30,000 lb
x c.g. location	373.3 in.
y c.g. location	0.0 in.
z c.g. location	96.0 in.
Pitch moment of inertia	91,200 slug-ft^2
Roll moment of inertia	14,300 slug-ft^2
Yaw moment of inertia	101,000 slug-ft^2
Product of inertia	0 slug-ft^2

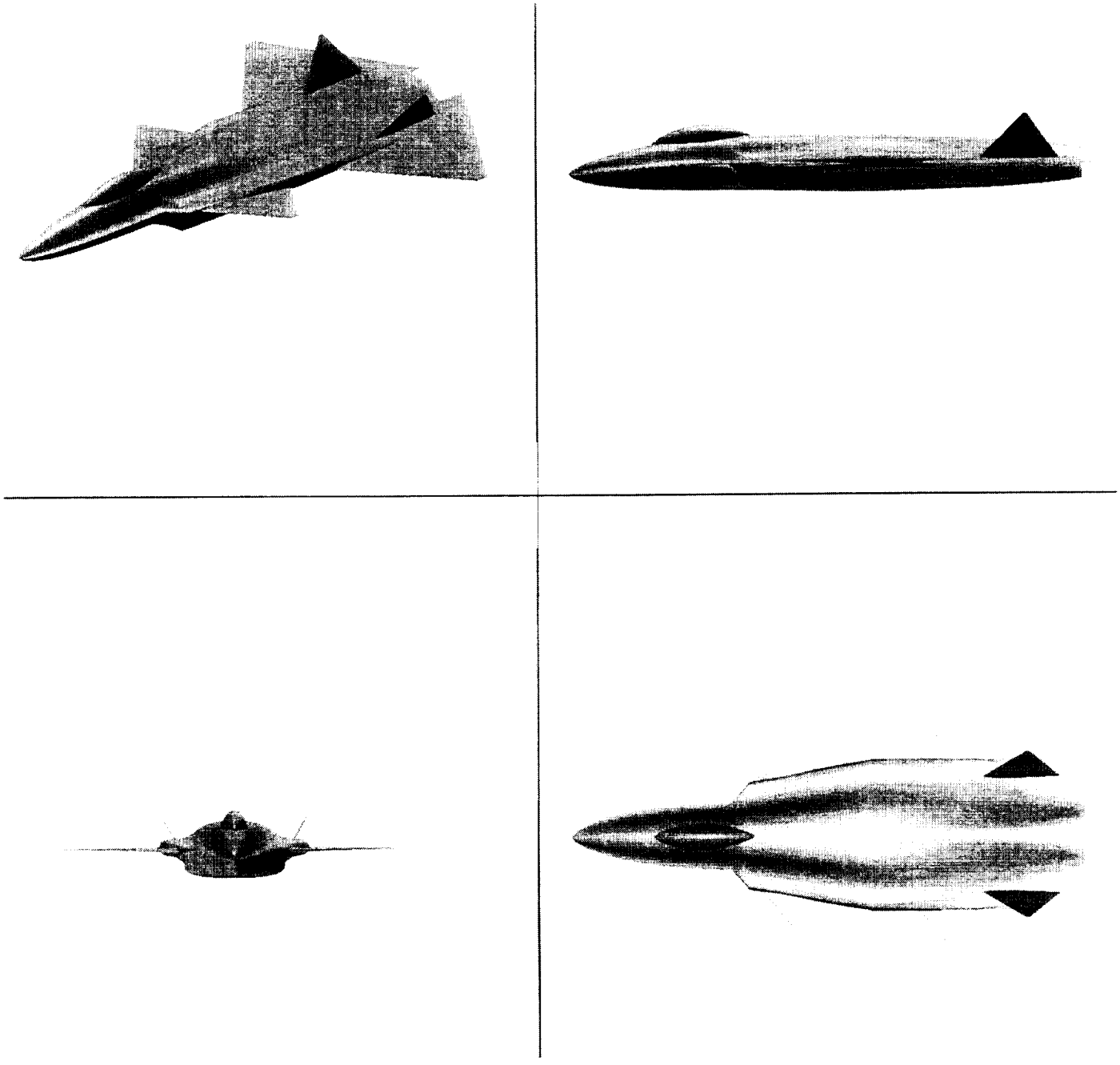

Figure 1. ASTOVL lift-fan aircraft

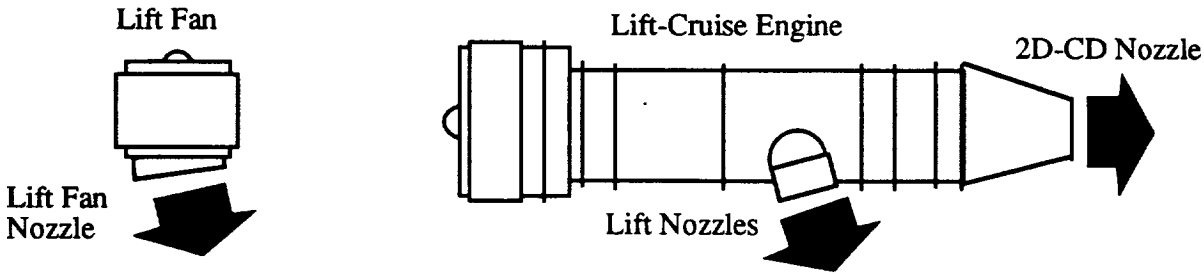

Figure 2. Propulsion system configuration

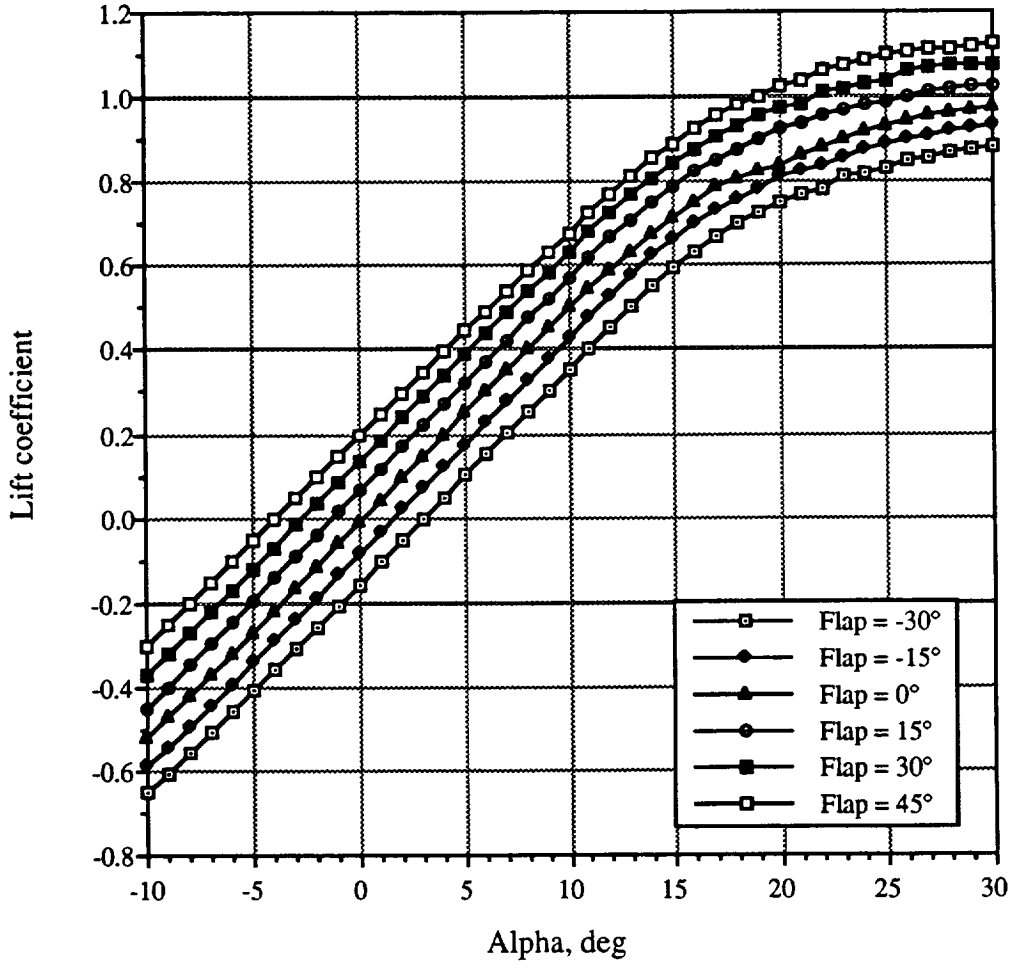

Figure 3. Lift coefficient for various flap deflections, M = 0.2

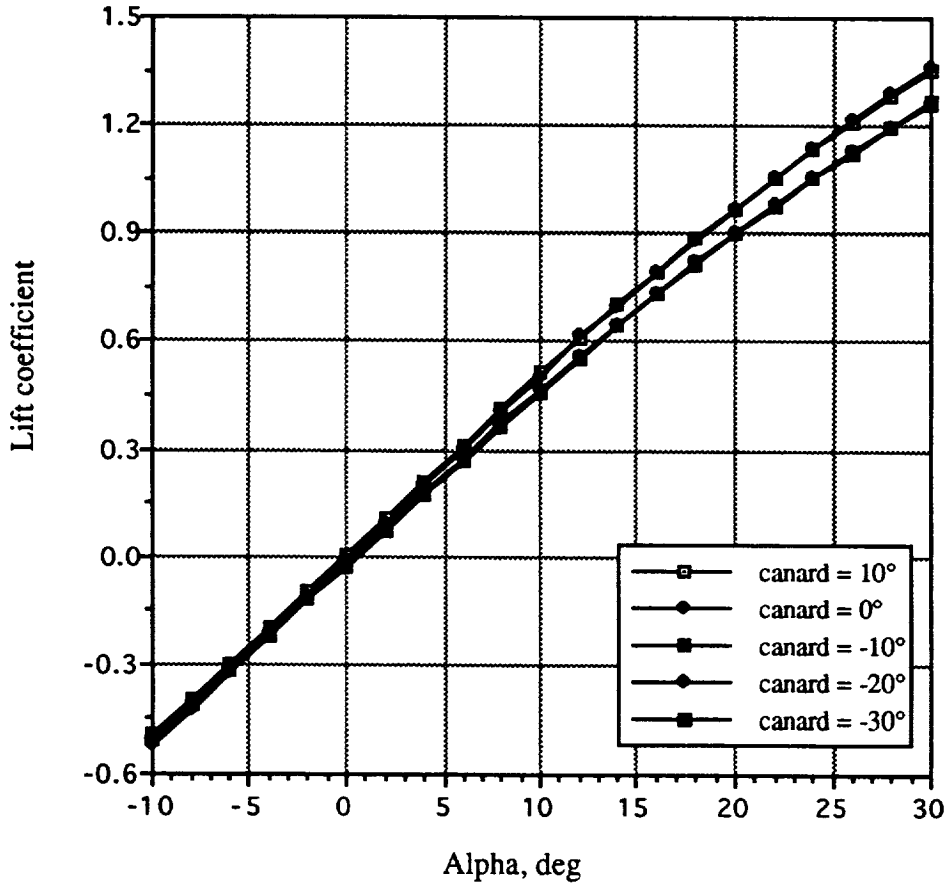

Figure 4. Lift coefficient for various canard deflections, M = 0.2

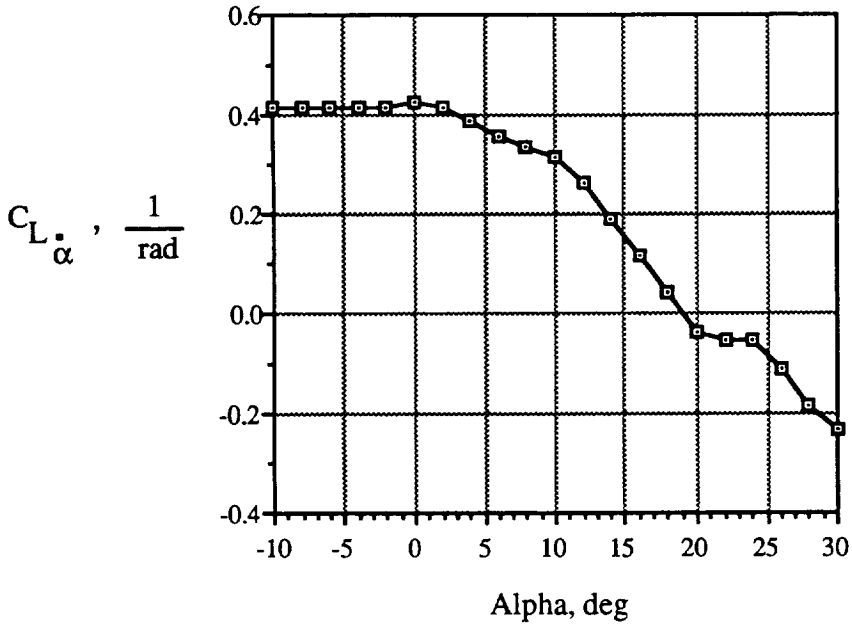

Figure 5. Lift coefficient due to angle-of-attack rate

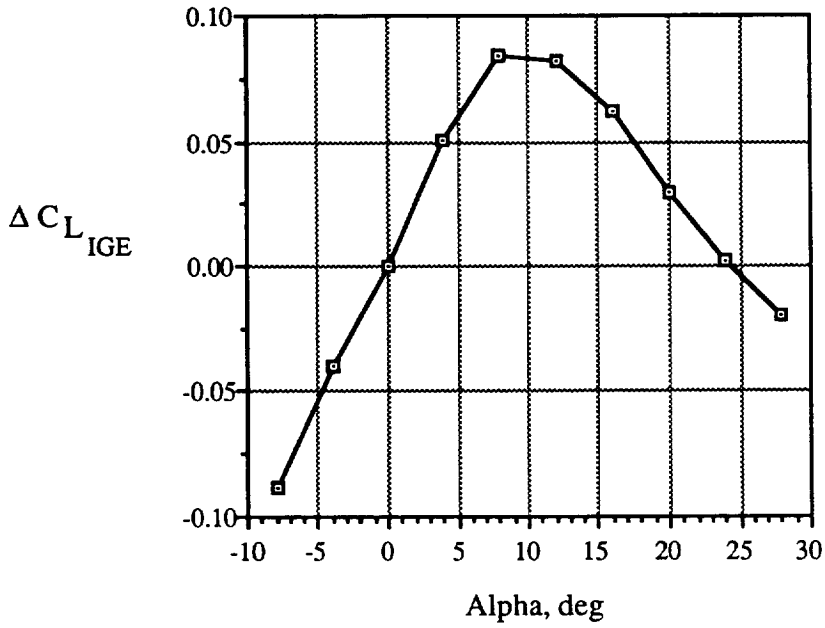

Figure 6. Lift coefficient increment due to ground plane influence

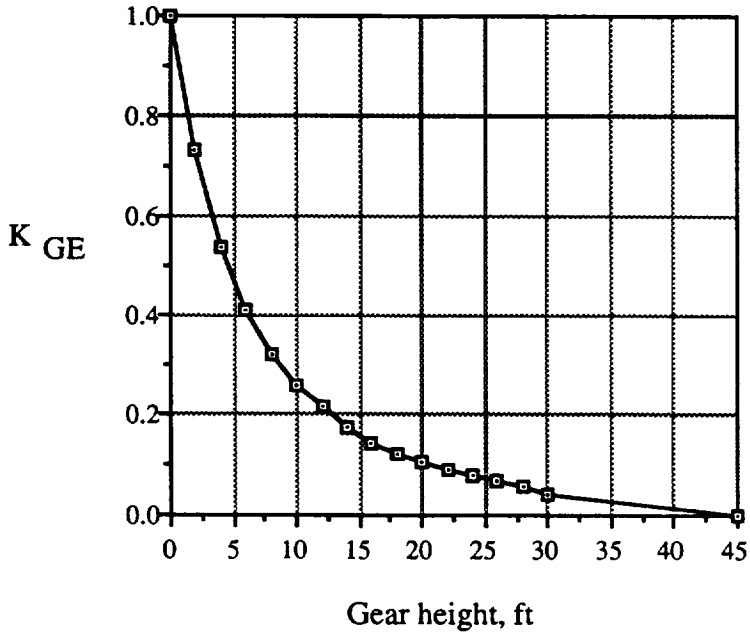

Figure 7. Power-off ground effect washout factor

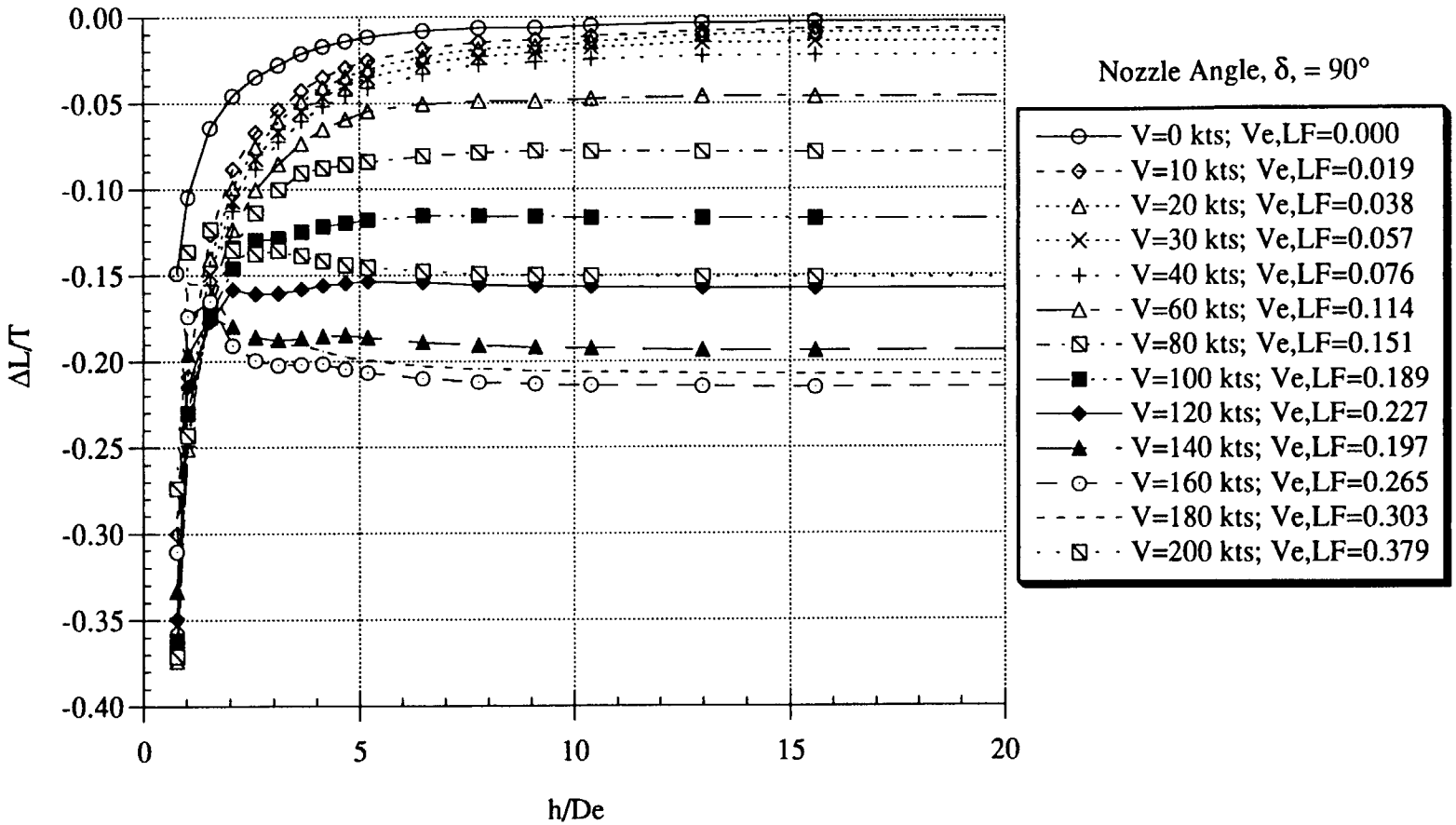

Figure 8. Jet-induced lift increment due to the lift fan for various forward velocities, lift-fan nozzle = 90°

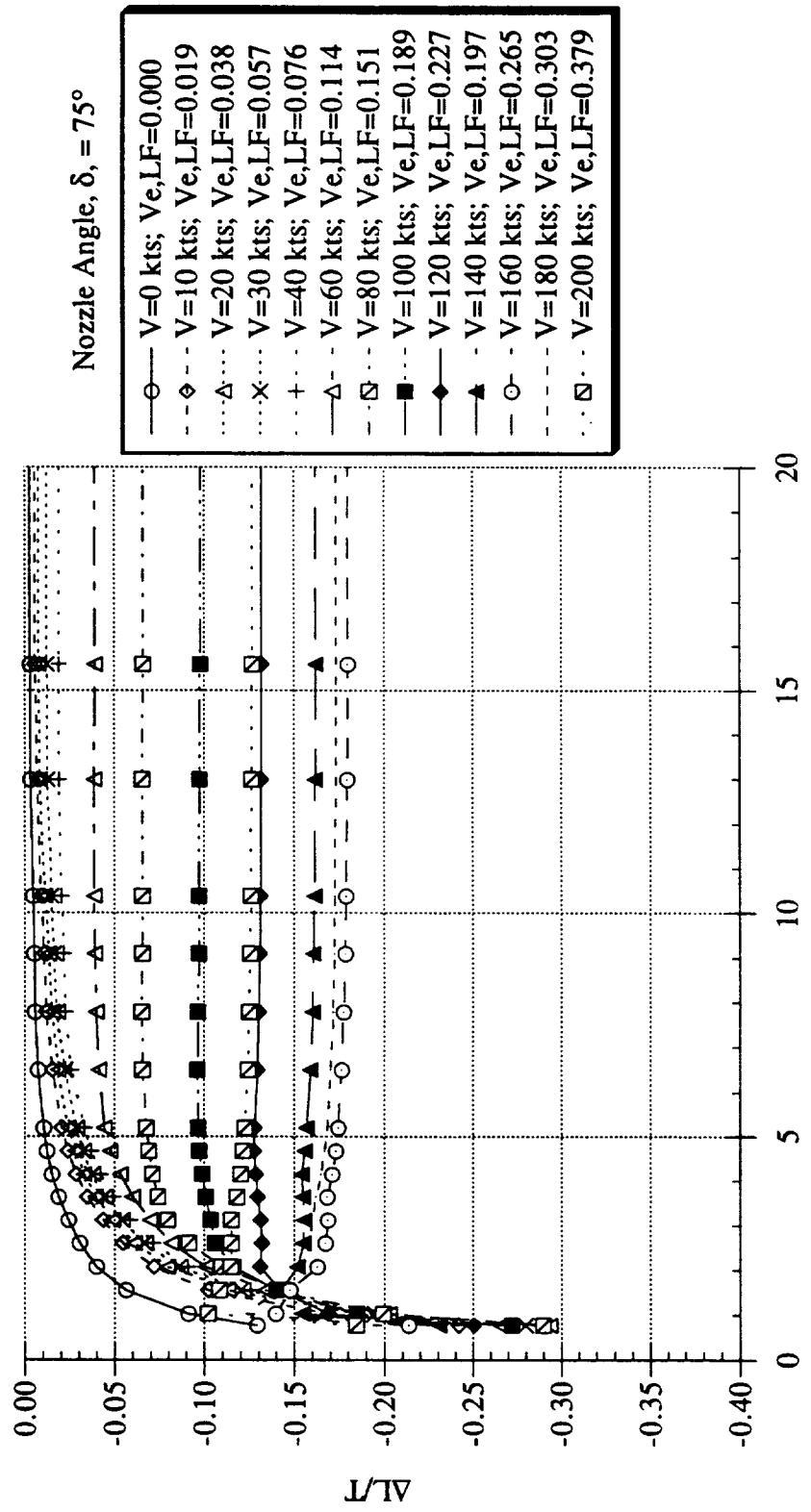

Figure 9. Jet-induced lift increment due to the lift fan for various forward velocities, lift-fan nozzle = 75°

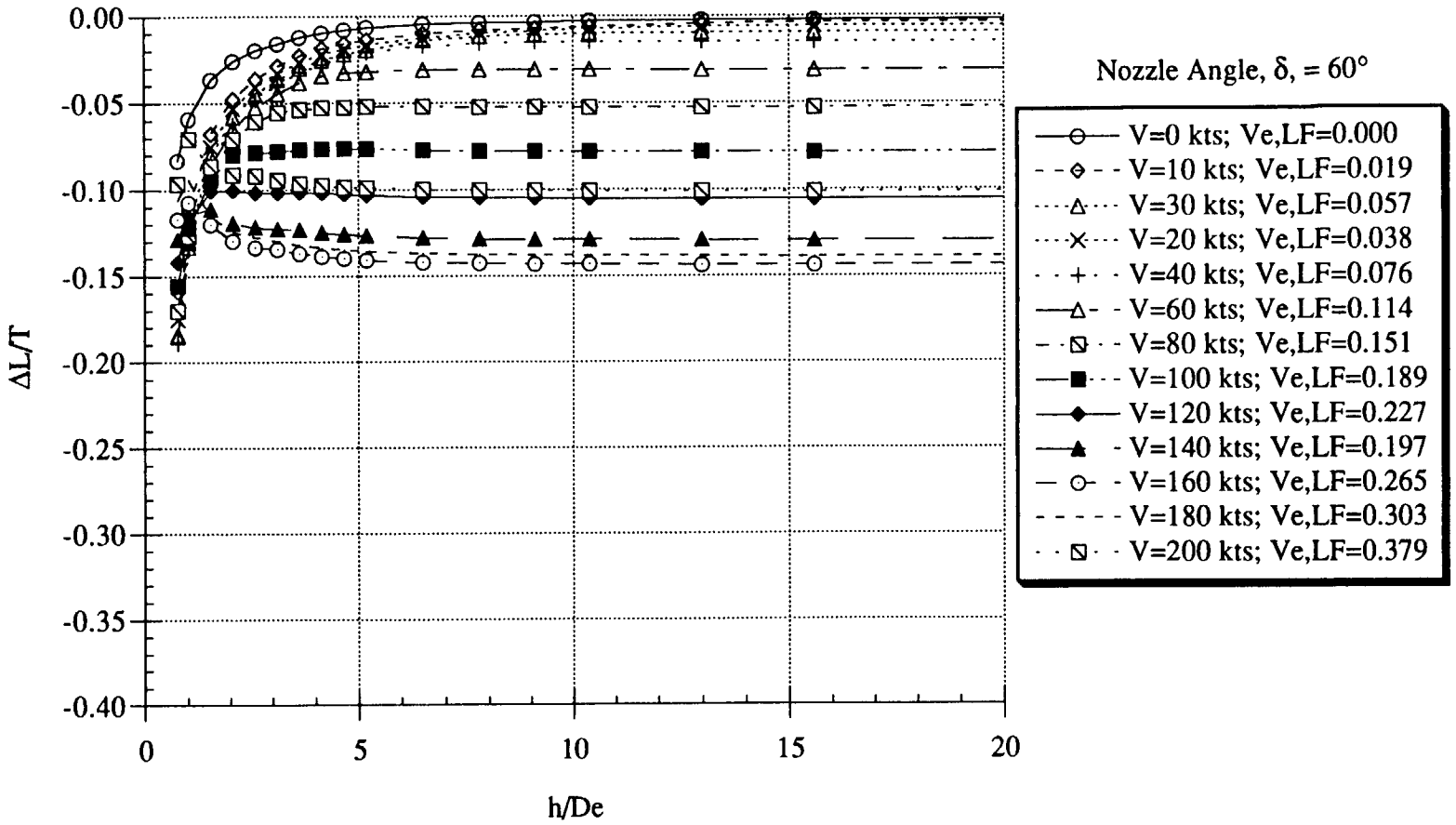

Figure 10. Jet-induced lift increment due to the lift fan for various forward velocities, lift-fan nozzle = 60°

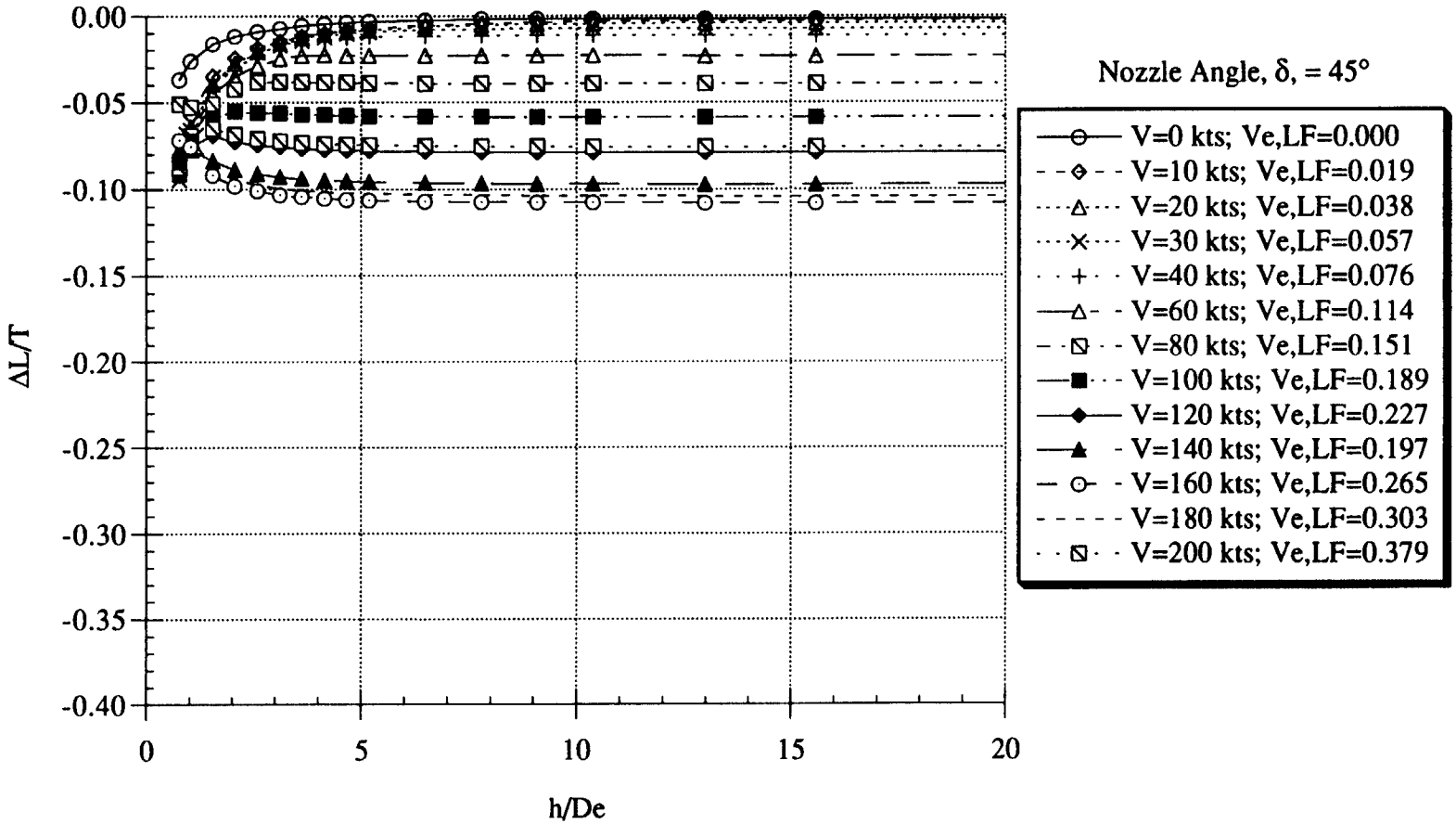

Figure 11. Jet-induced lift increment due to the lift fan for various forward velocities, lift-fan nozzle = 45°

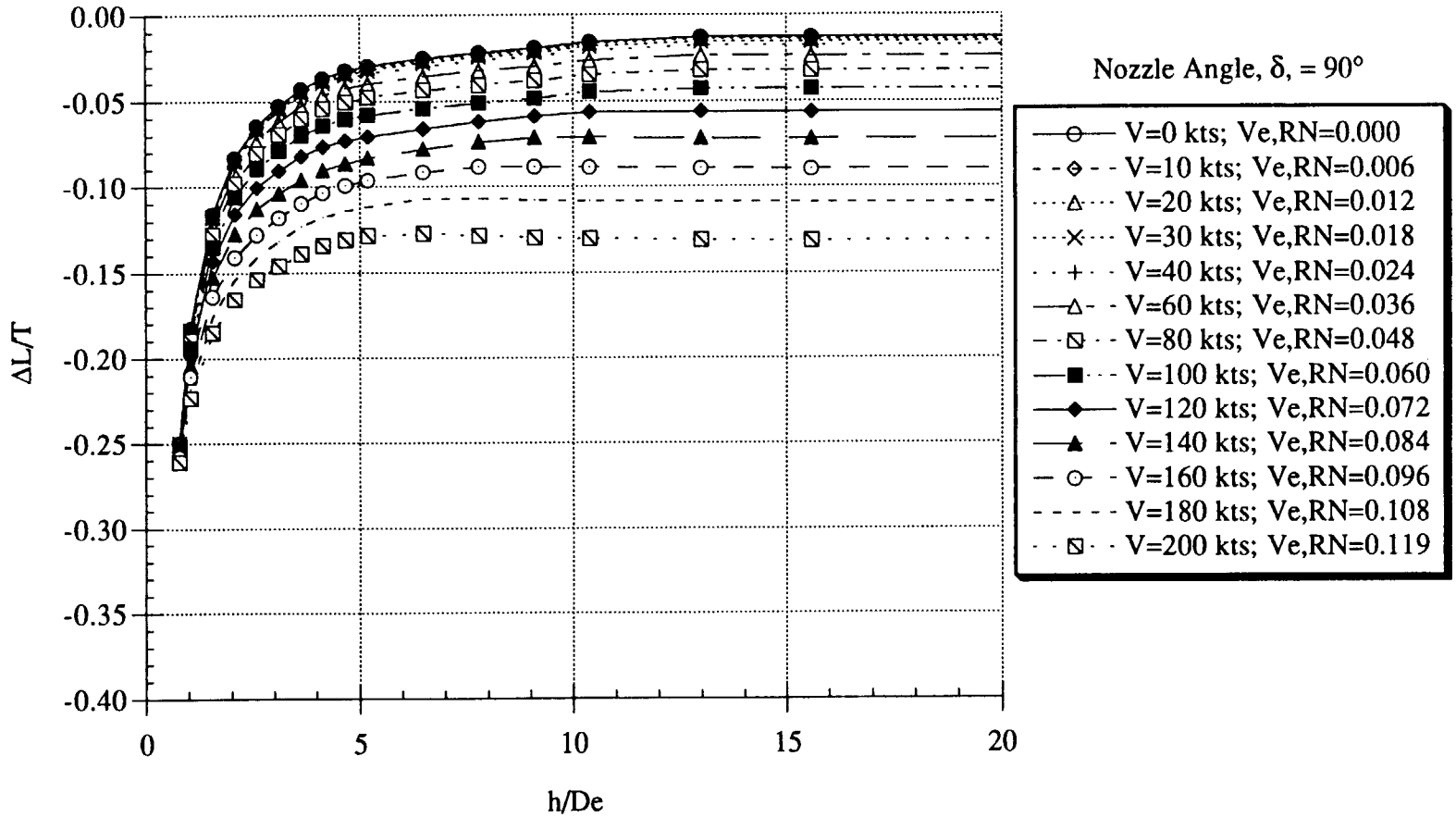

Figure 12. Jet-induced lift increment due to the lift nozzles for various forward velocities, lift nozzles = 90°

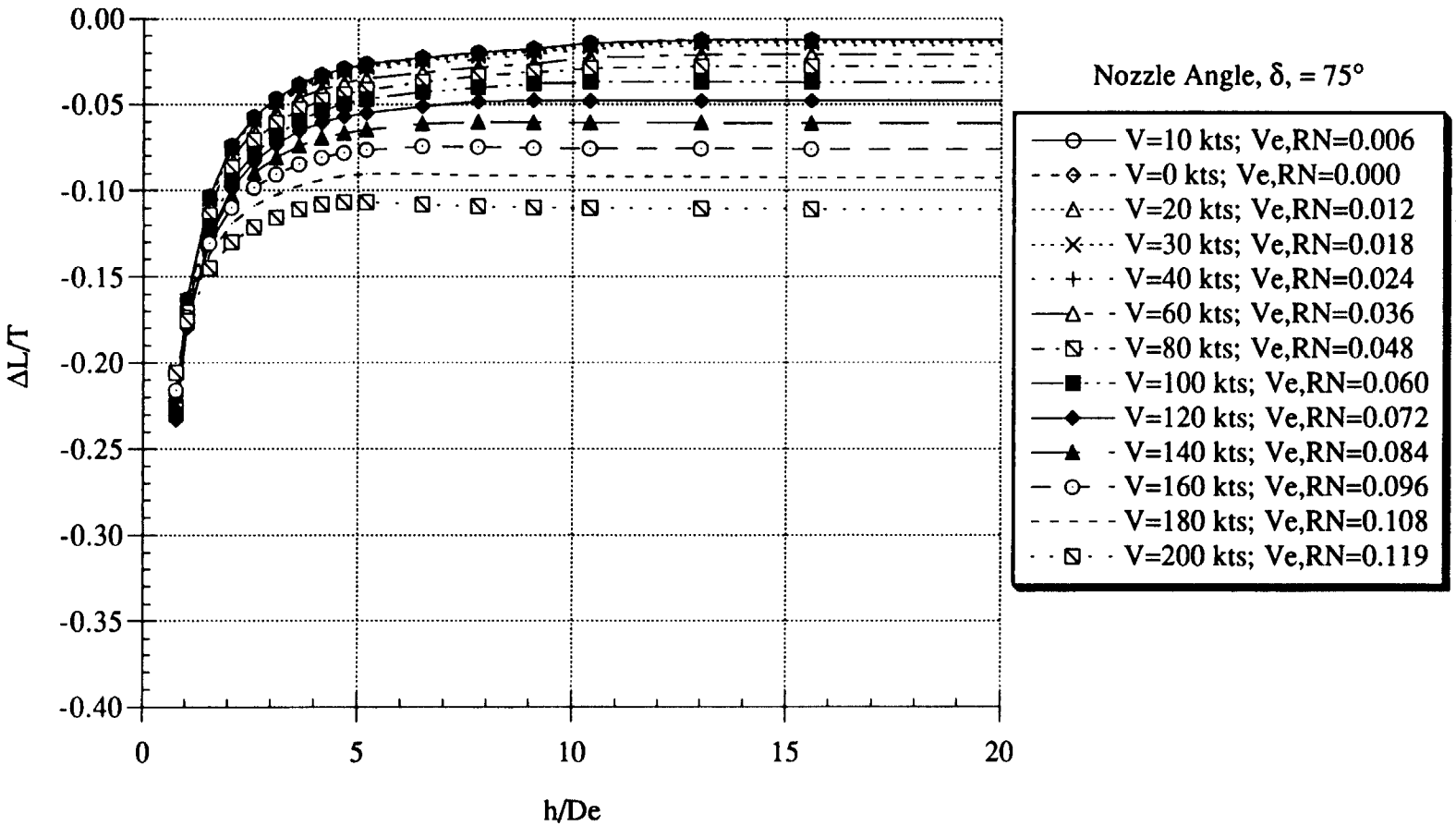

Figure 13. Jet-induced lift increment due to the lift nozzles for various forward velocities, lift nozzles = 75°

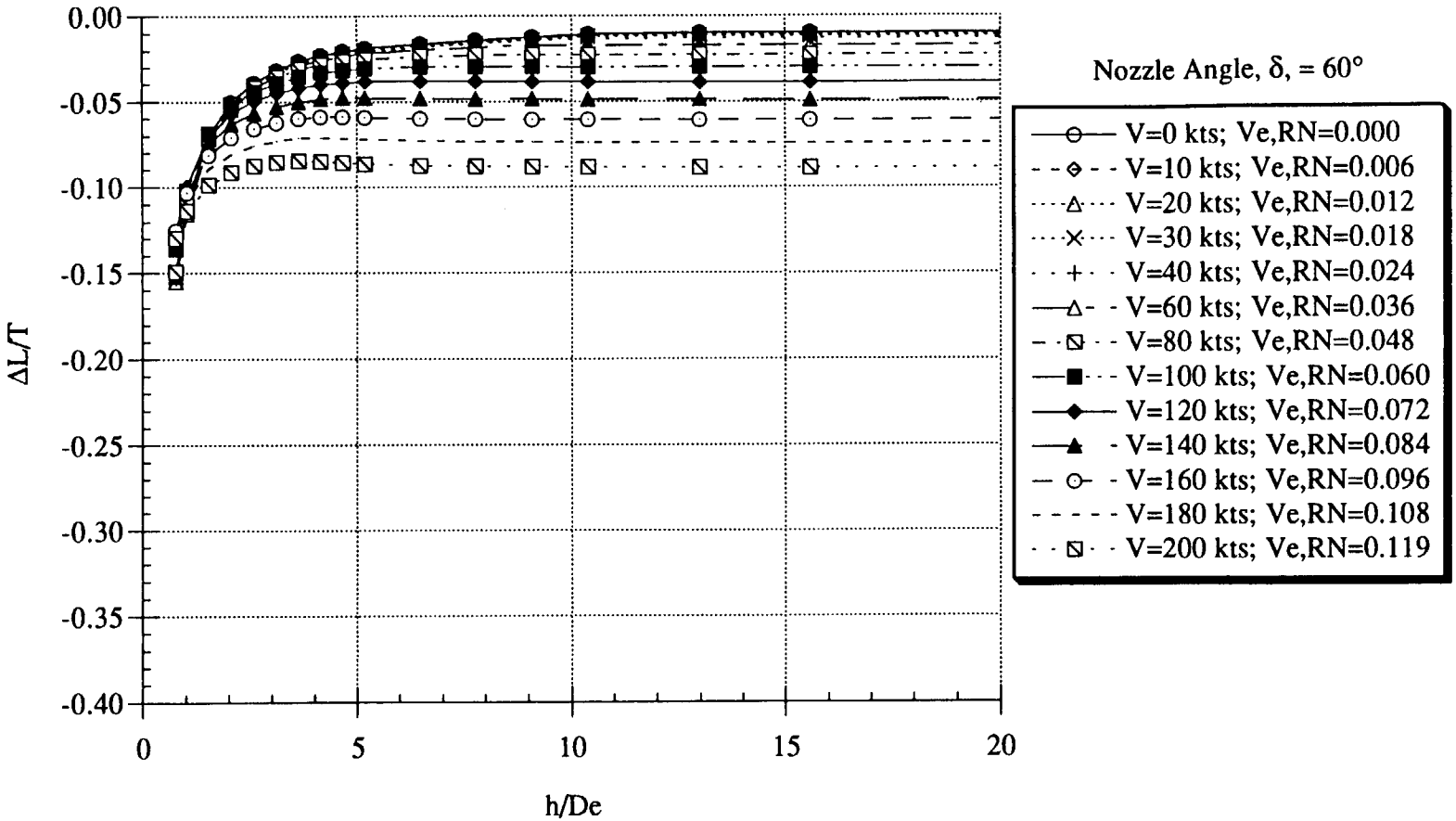

Figure 14. Jet-induced lift increment due to the lift nozzles for various forward velocities, lift nozzles = 60°

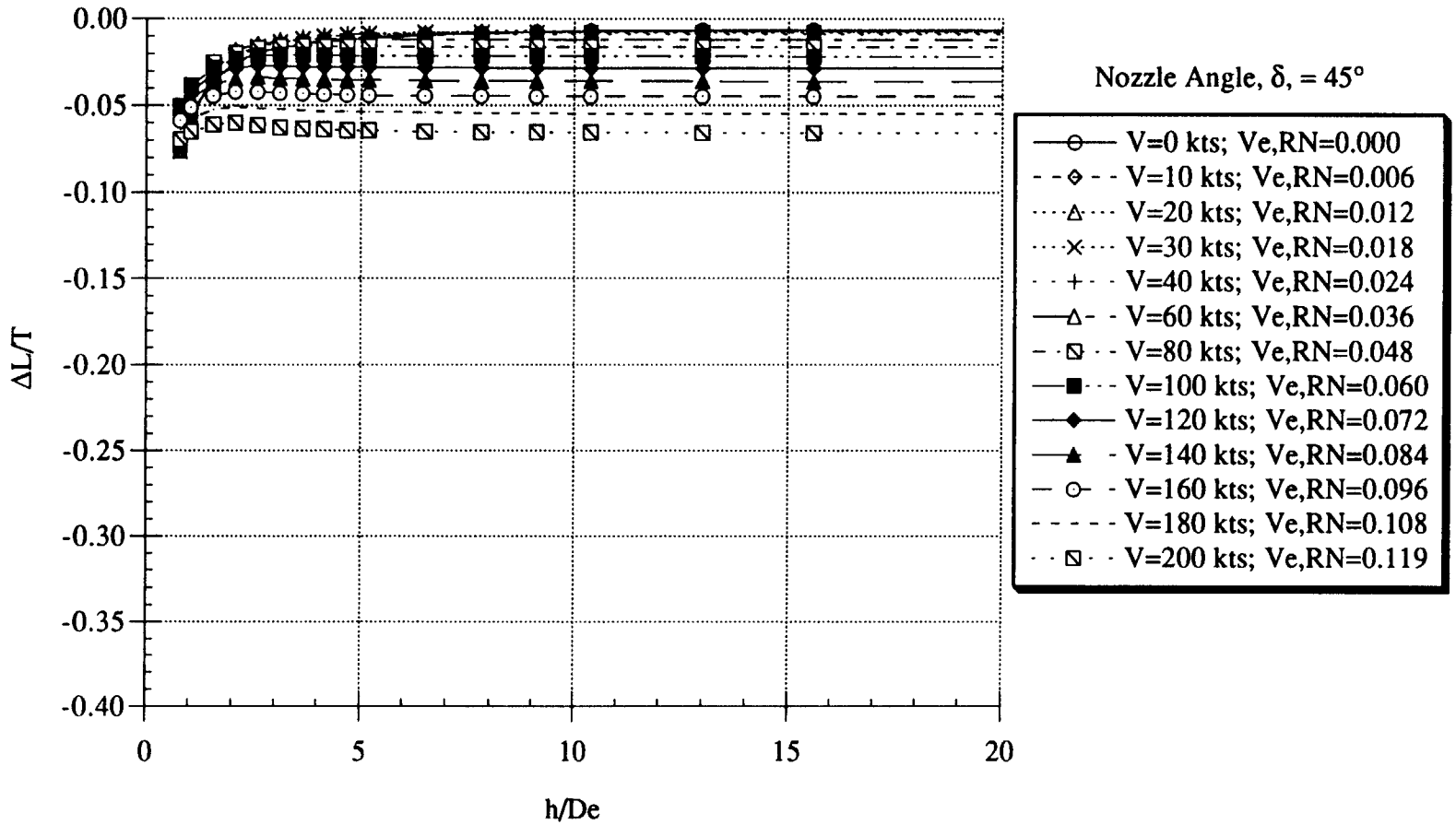

Figure 15. Jet-induced lift increment due to the lift nozzles for various forward velocities, lift nozzles = 45°

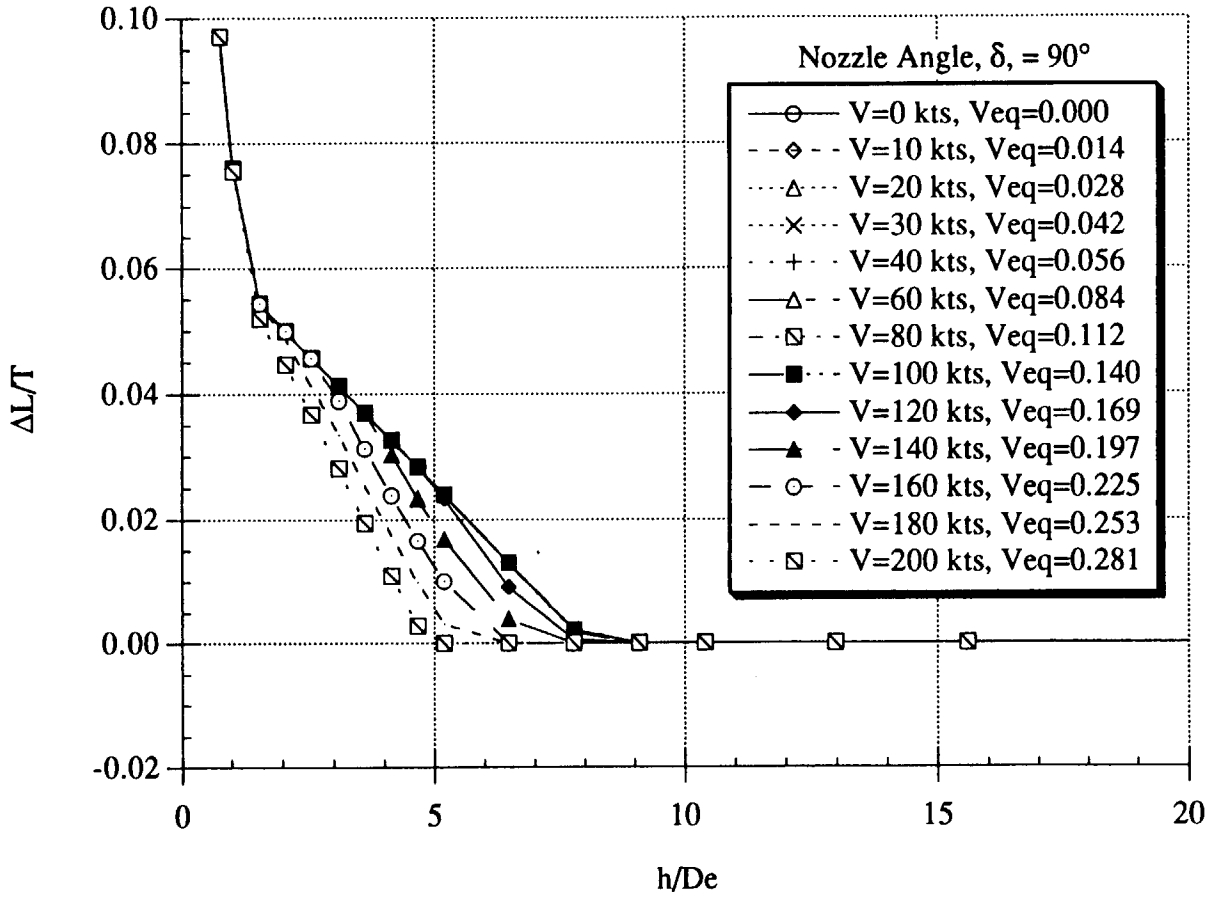

Figure 16. Jet-induced lift increment due to the fountain for various forward velocities, equivalent lift-fan and lift nozzles = 90°

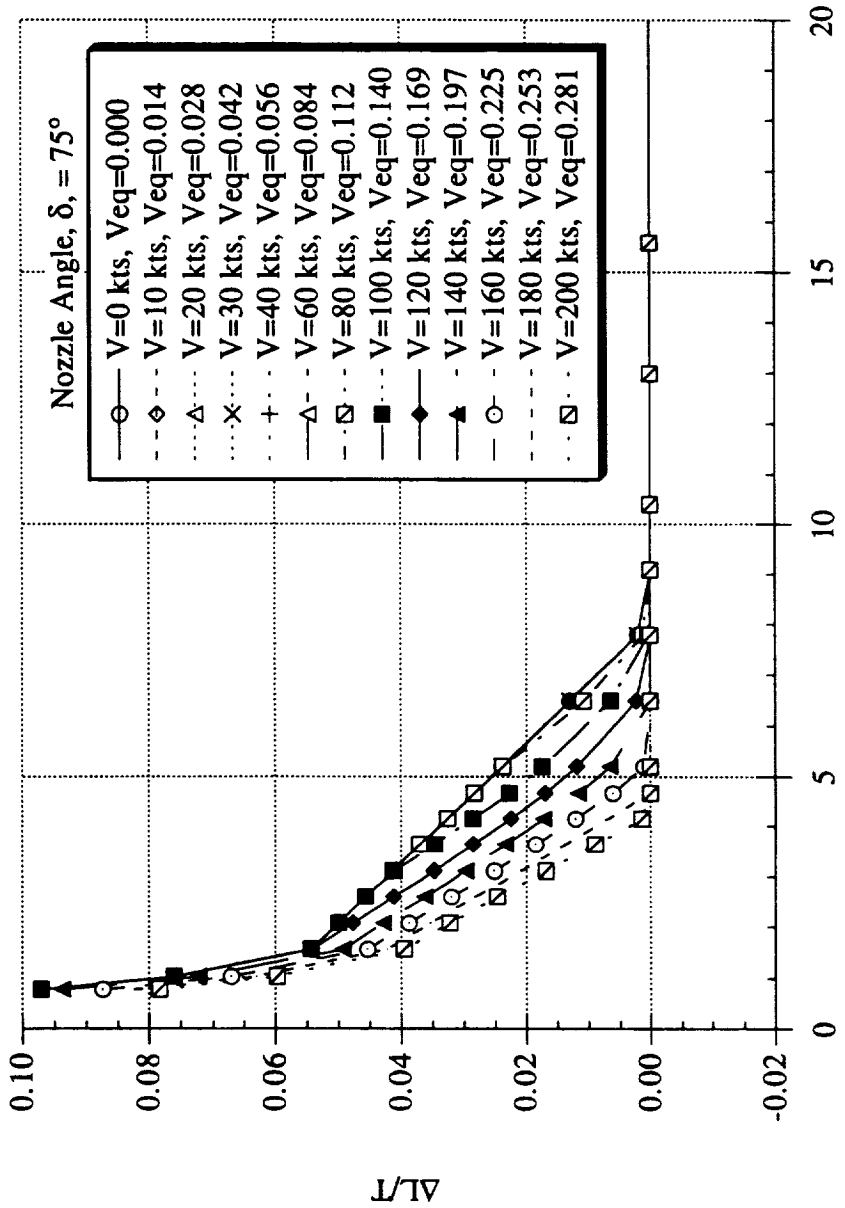

Figure 17. Jet-induced lift increment due to the fountain for various forward velocities, equivalent lift-fan and lift nozzles = 75°

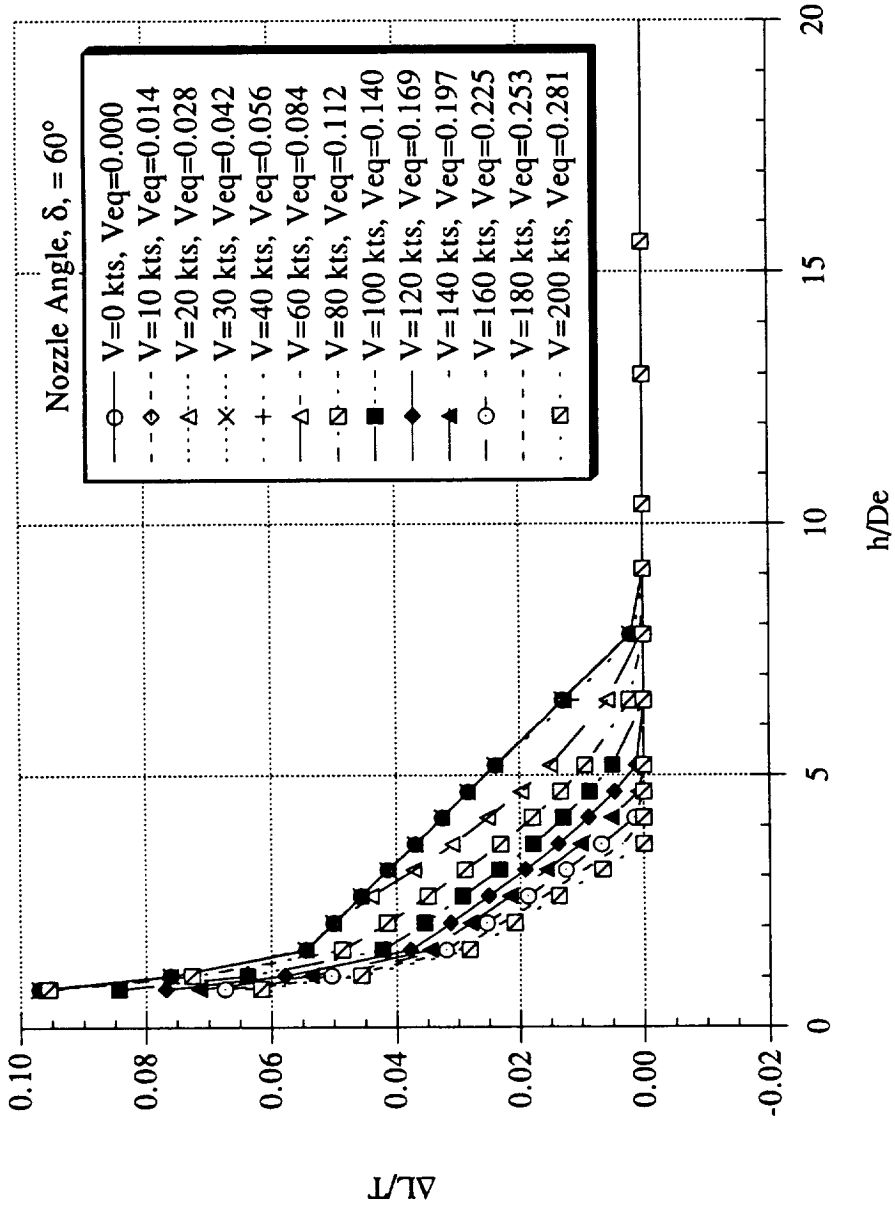

Figure 18. Jet-induced lift increment due to the fountain for various forward velocities, equivalent lift-fan and lift nozzles = 60°

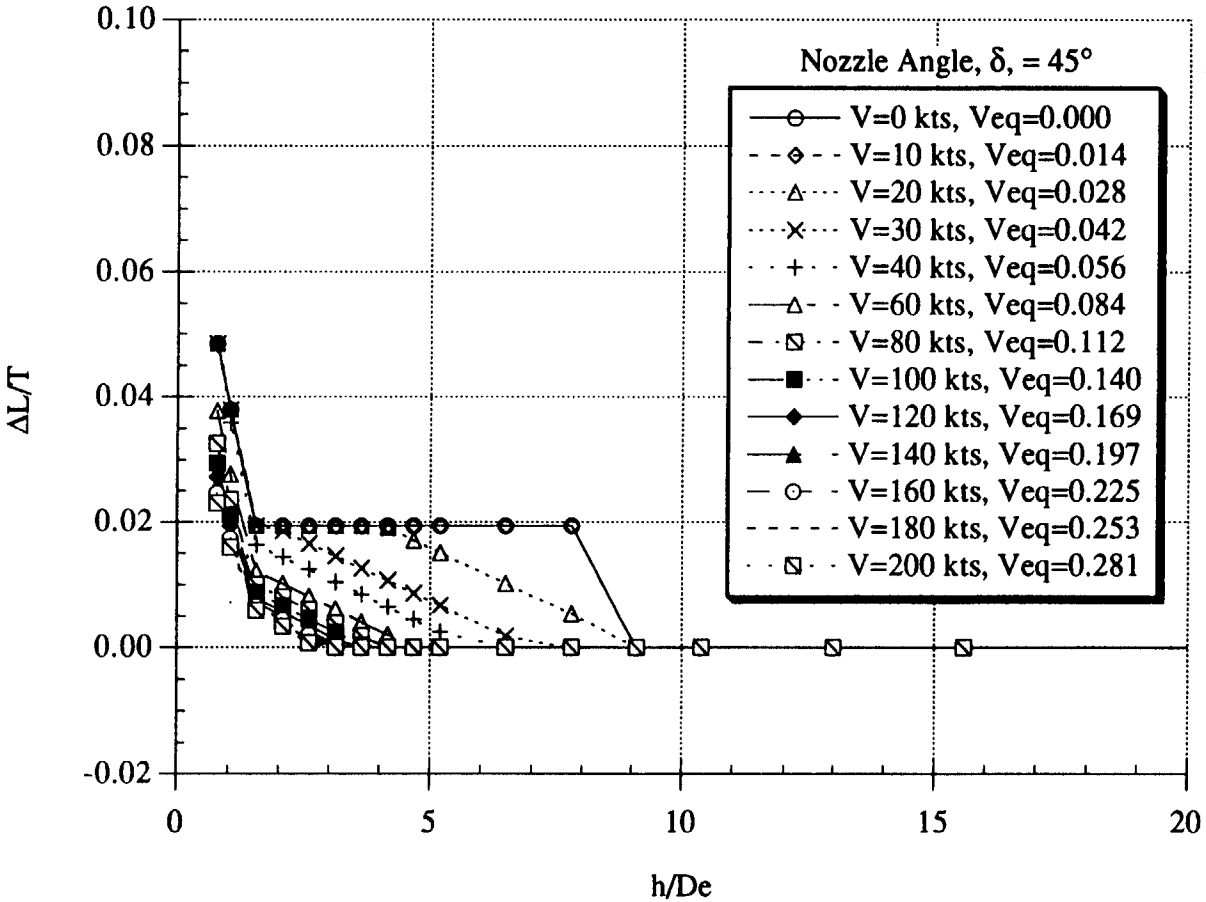

Figure 19. Jet-induced lift increment due to the fountain for various forward velocities, equivalent lift-fan and lift nozzles = 45°

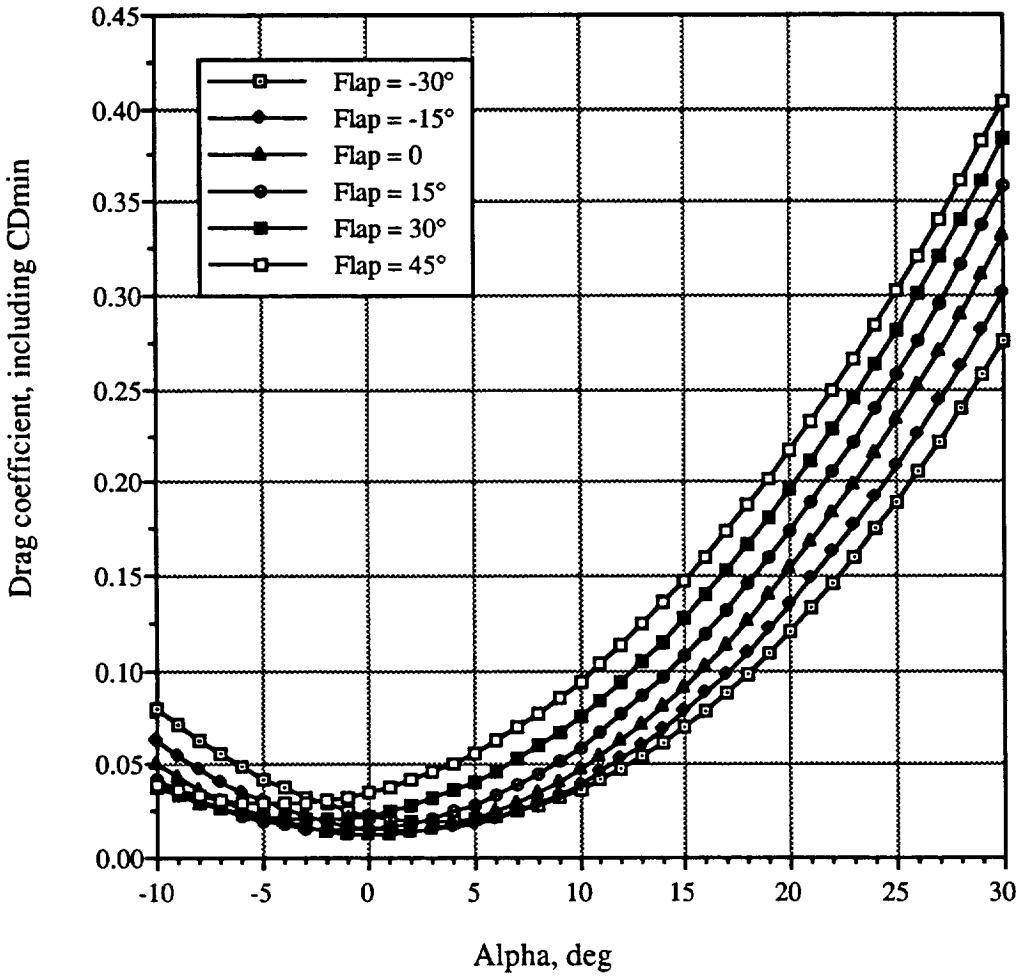

Figure 20. Drag coefficient for various flap deflections (includes CDmin), M = 0.2

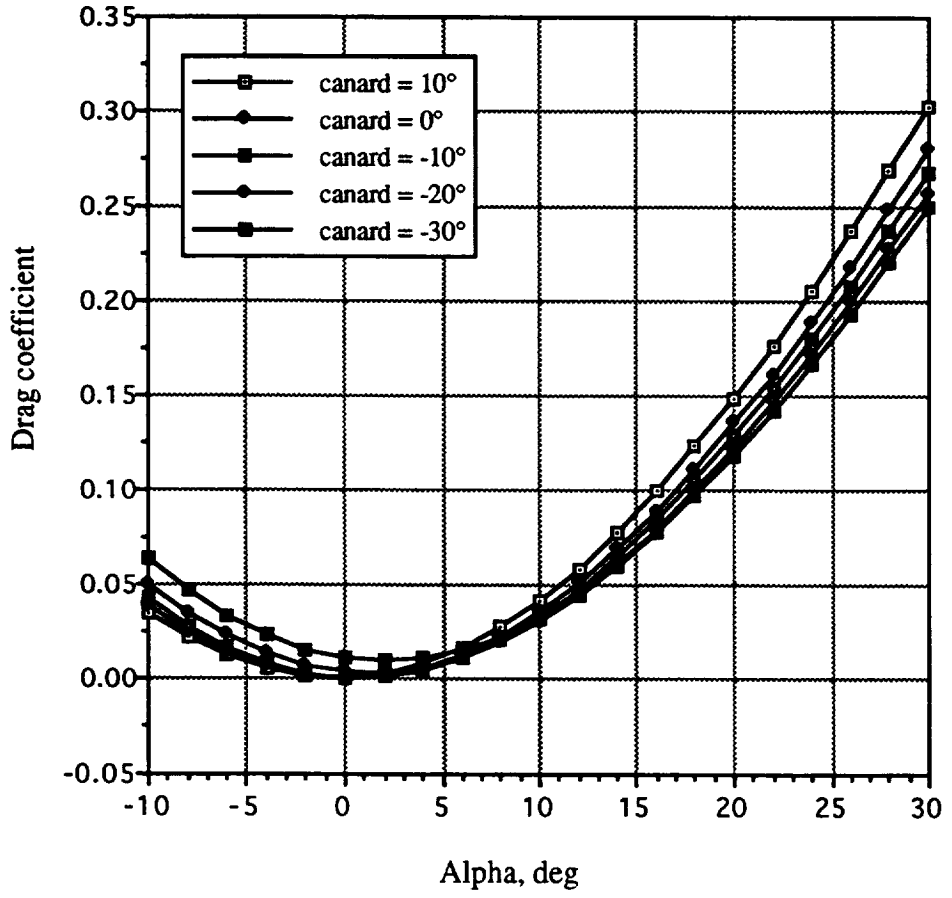

Figure 21. Drag coefficient for various canard deflections, M = 0.2

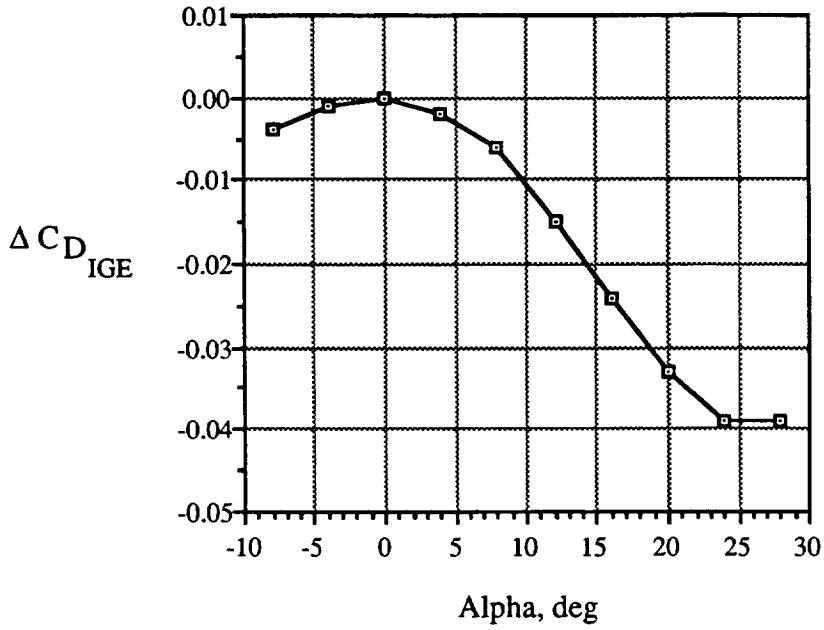

Figure 22. Drag coefficient increment due to ground plane influence

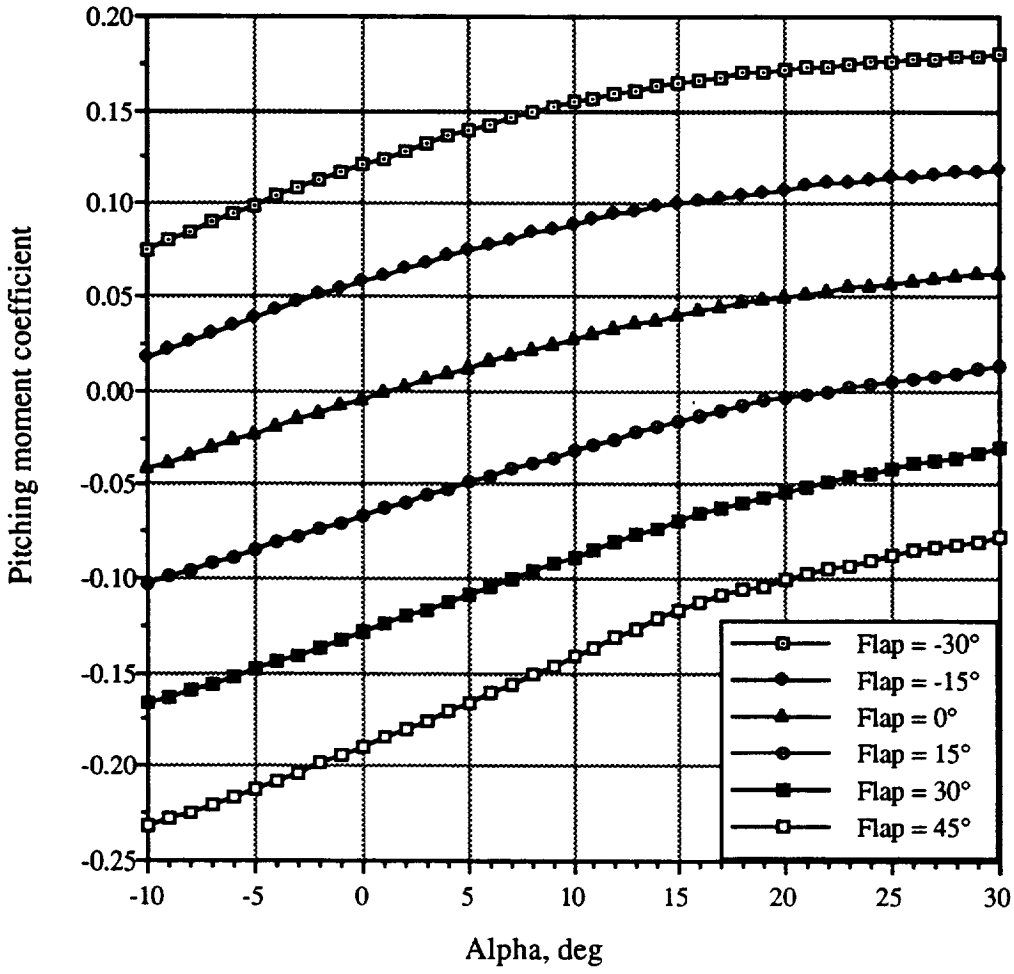

Figure 23. Pitching moment coefficient for various flap deflections, M = 0.2

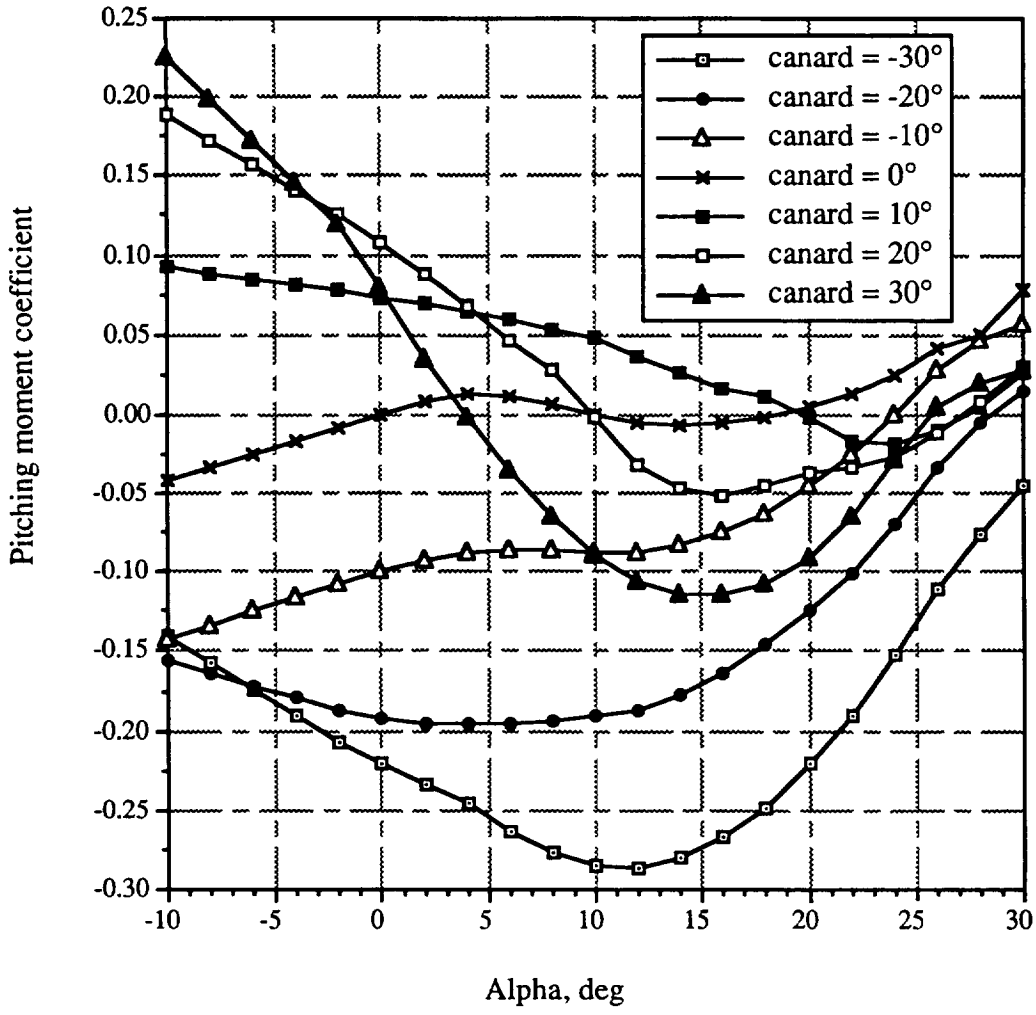

Figure 24. Pitching moment coefficient for various canard deflections, M = 0.2

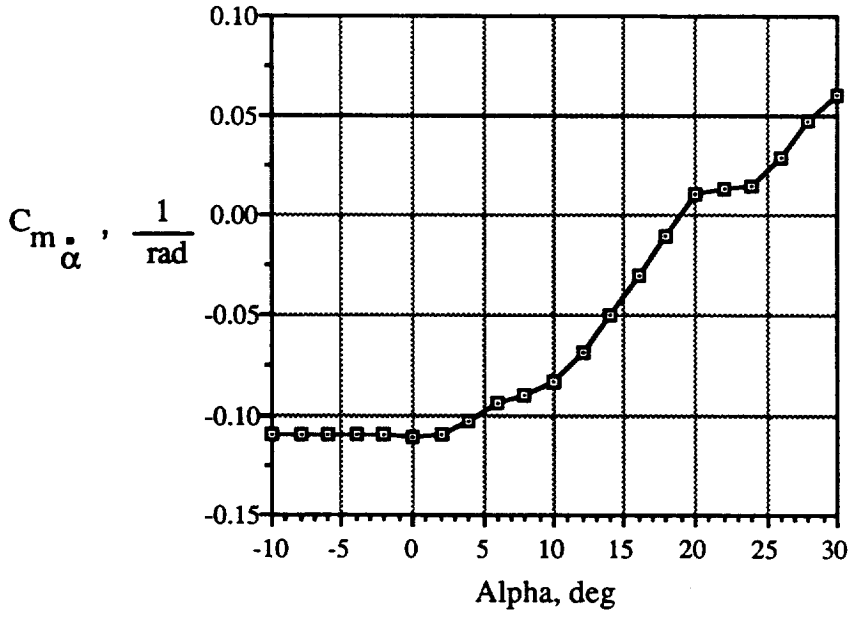

Figure 25. Pitching moment coefficient due to angle-of-attack rate

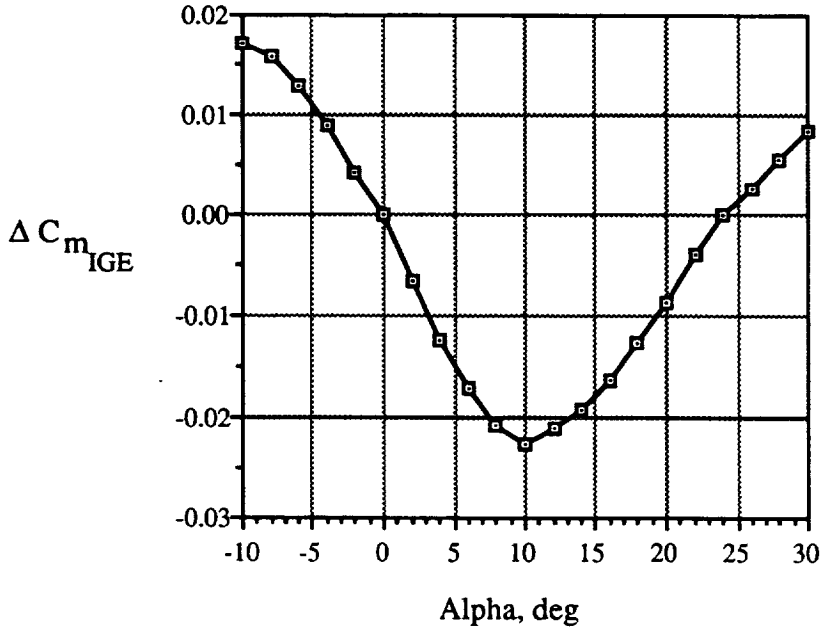

Figure 26. Pitching moment coefficient increment due to ground plane influence

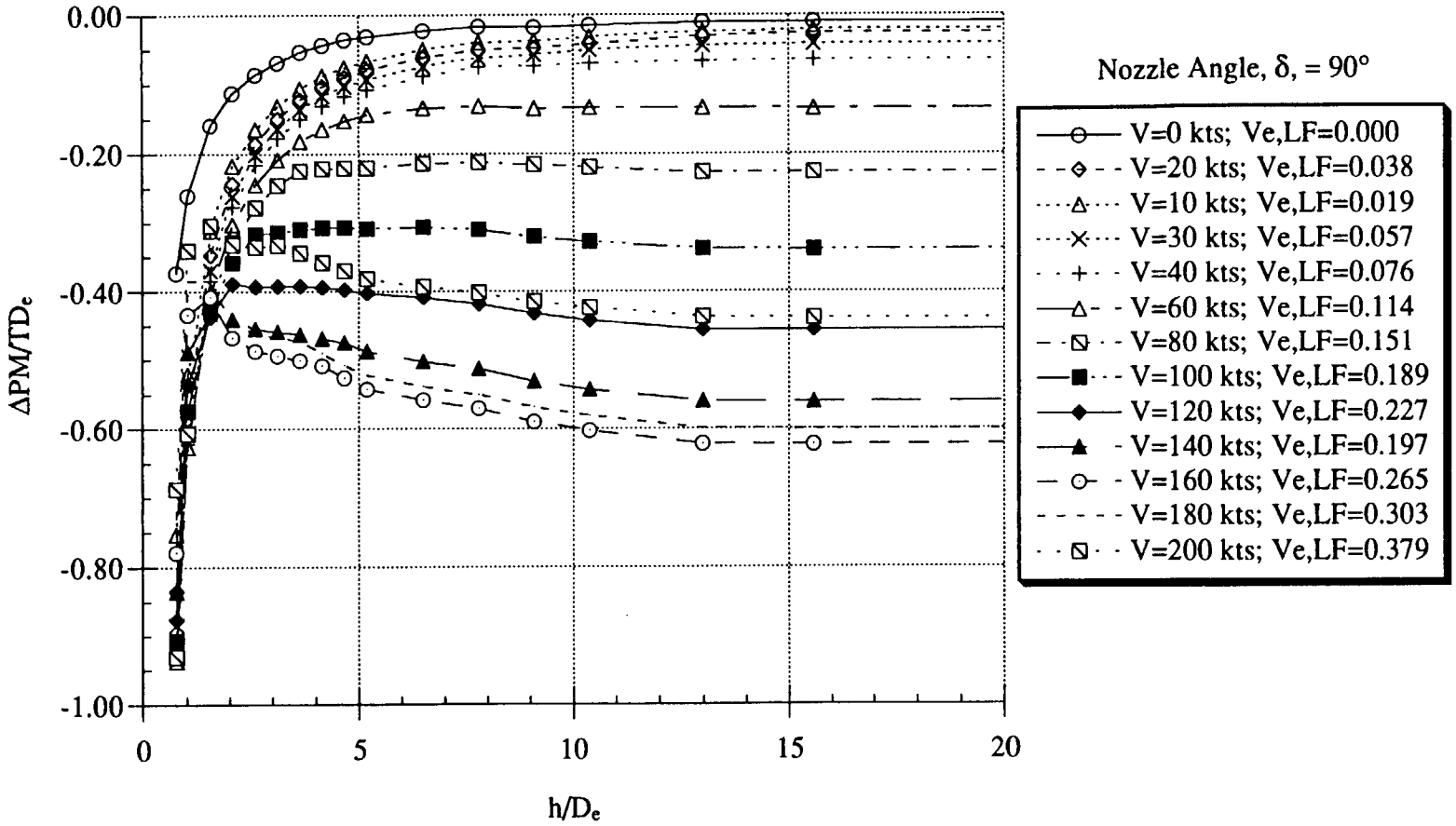

Figure 27. Jet-induced pitching moment increment due to the lift fan for various forward velocities, lift-fan nozzle = 90°

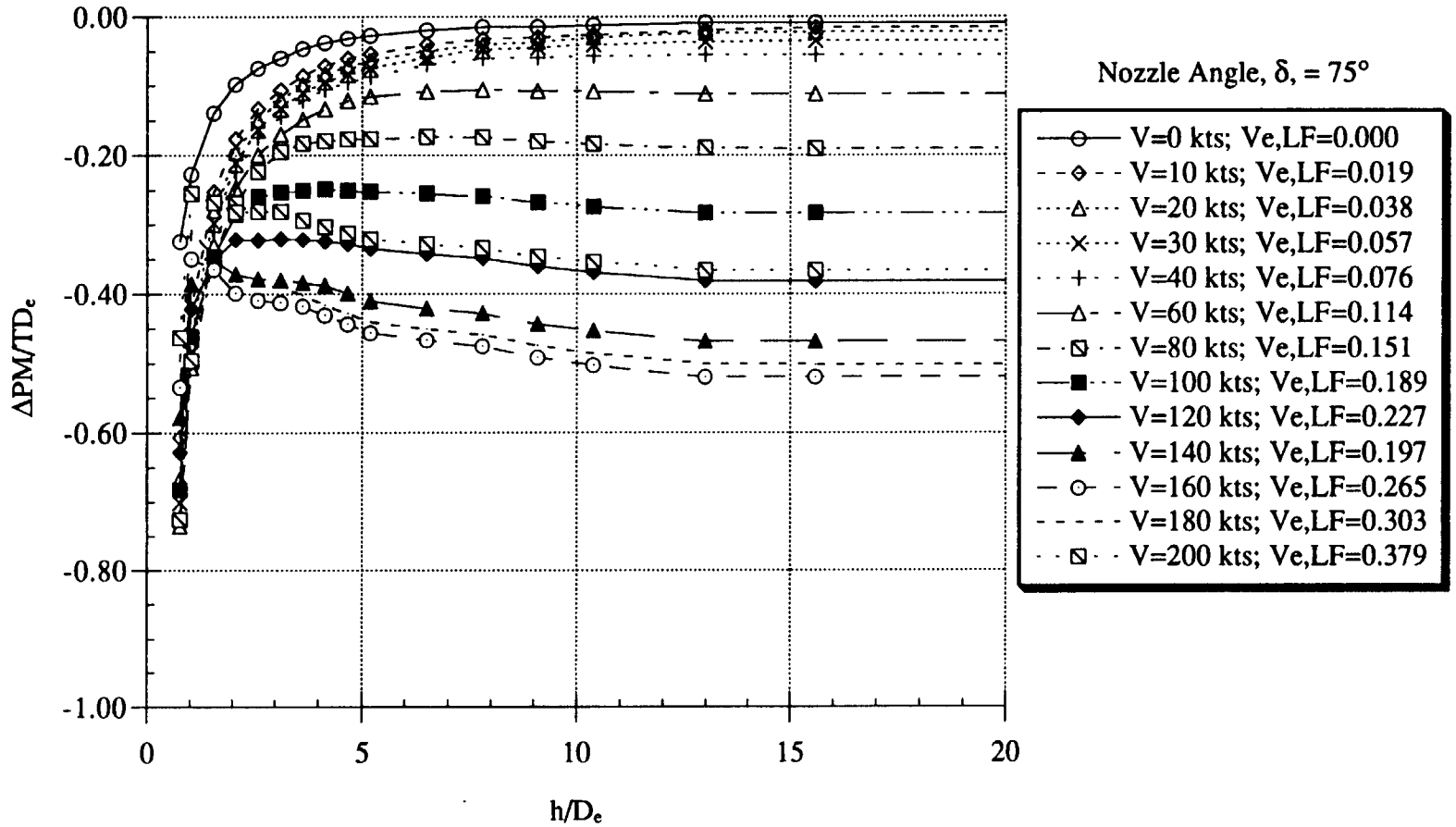

Figure 28. Jet-induced pitching moment increment due to the lift fan for various forward velocities, lift-fan nozzle = 75°

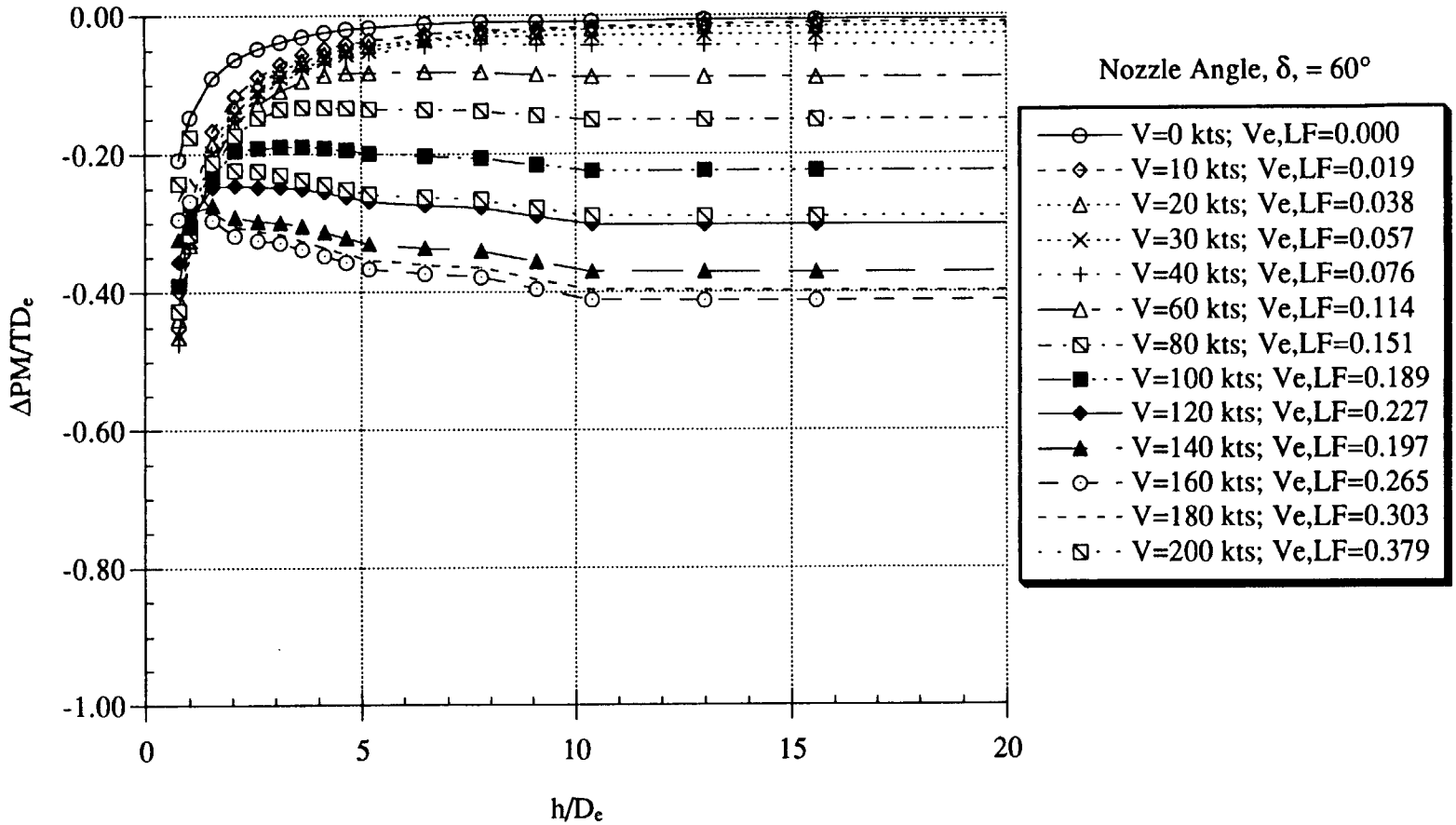

Figure 29. Jet-induced pitching moment increment due to the lift fan for various forward velocities, lift-fan nozzle = 60°

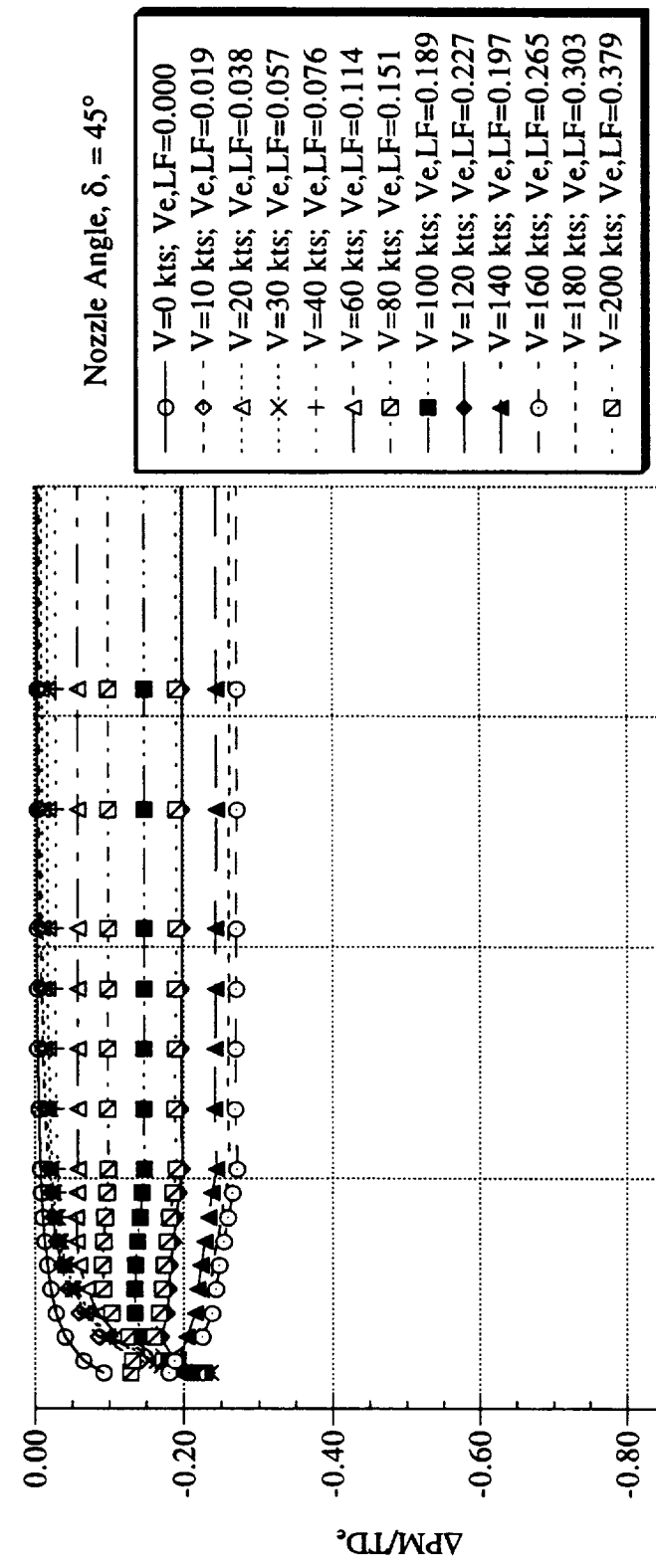

Figure 30. Jet-induced pitching moment increment due to the lift fan for various forward velocities, lift-fan nozzle = 45°

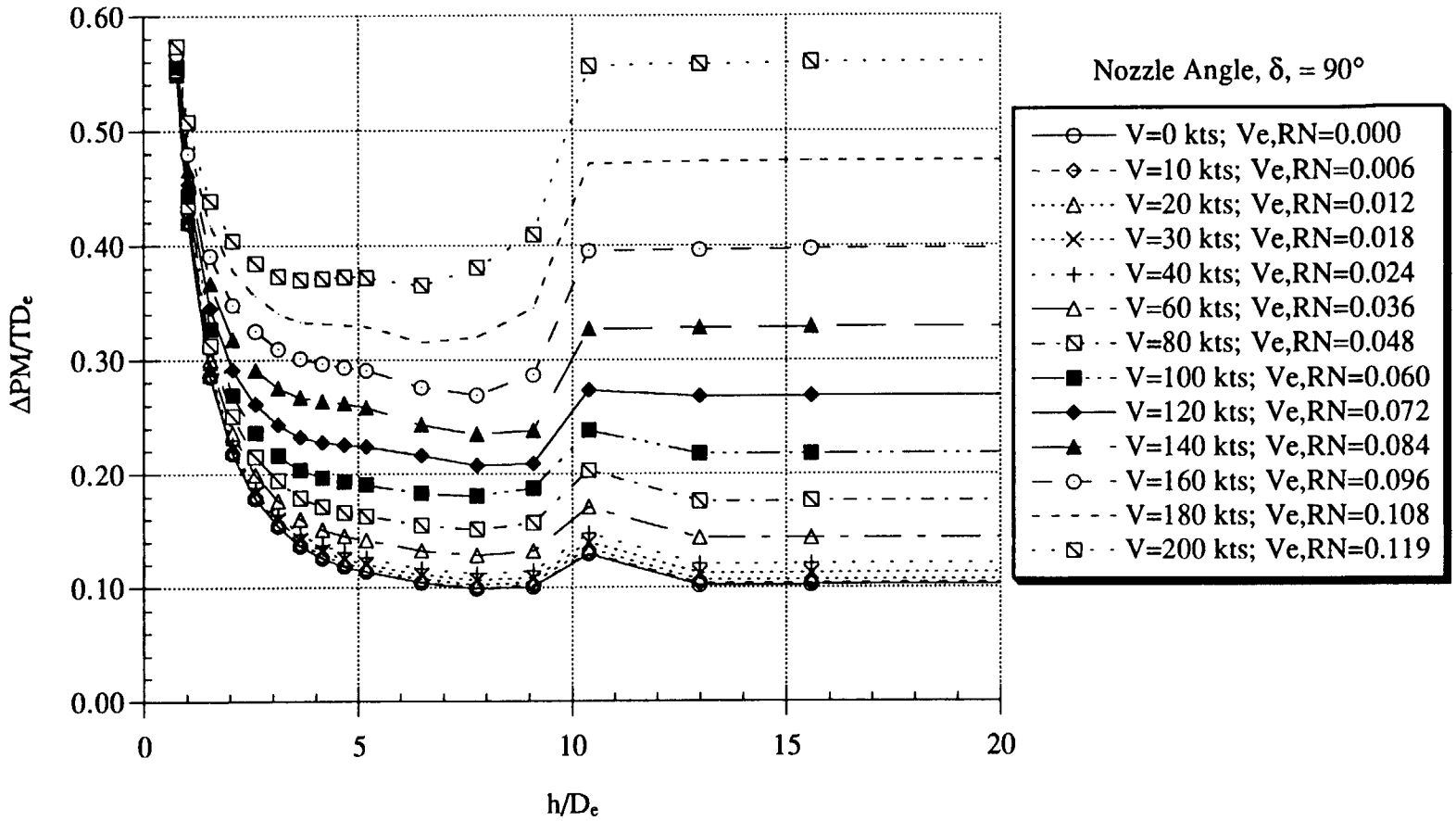

Figure 31. Jet-induced pitching moment increment due to the lift nozzles for various forward velocities, lift nozzles = 90°

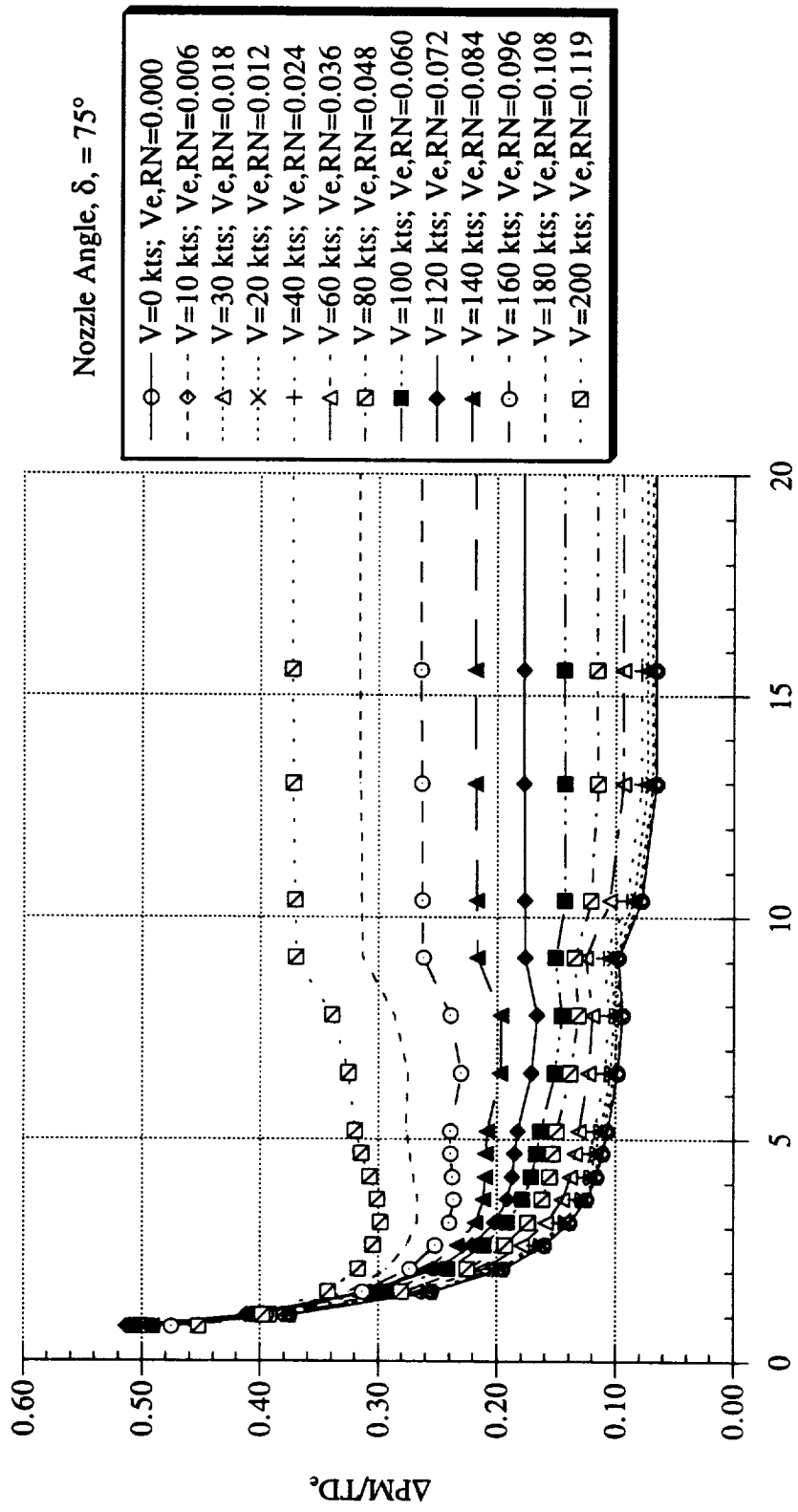

Figure 32. Jet-induced pitching moment increment due to the lift nozzles for various forward velocities, lift nozzles = 75°

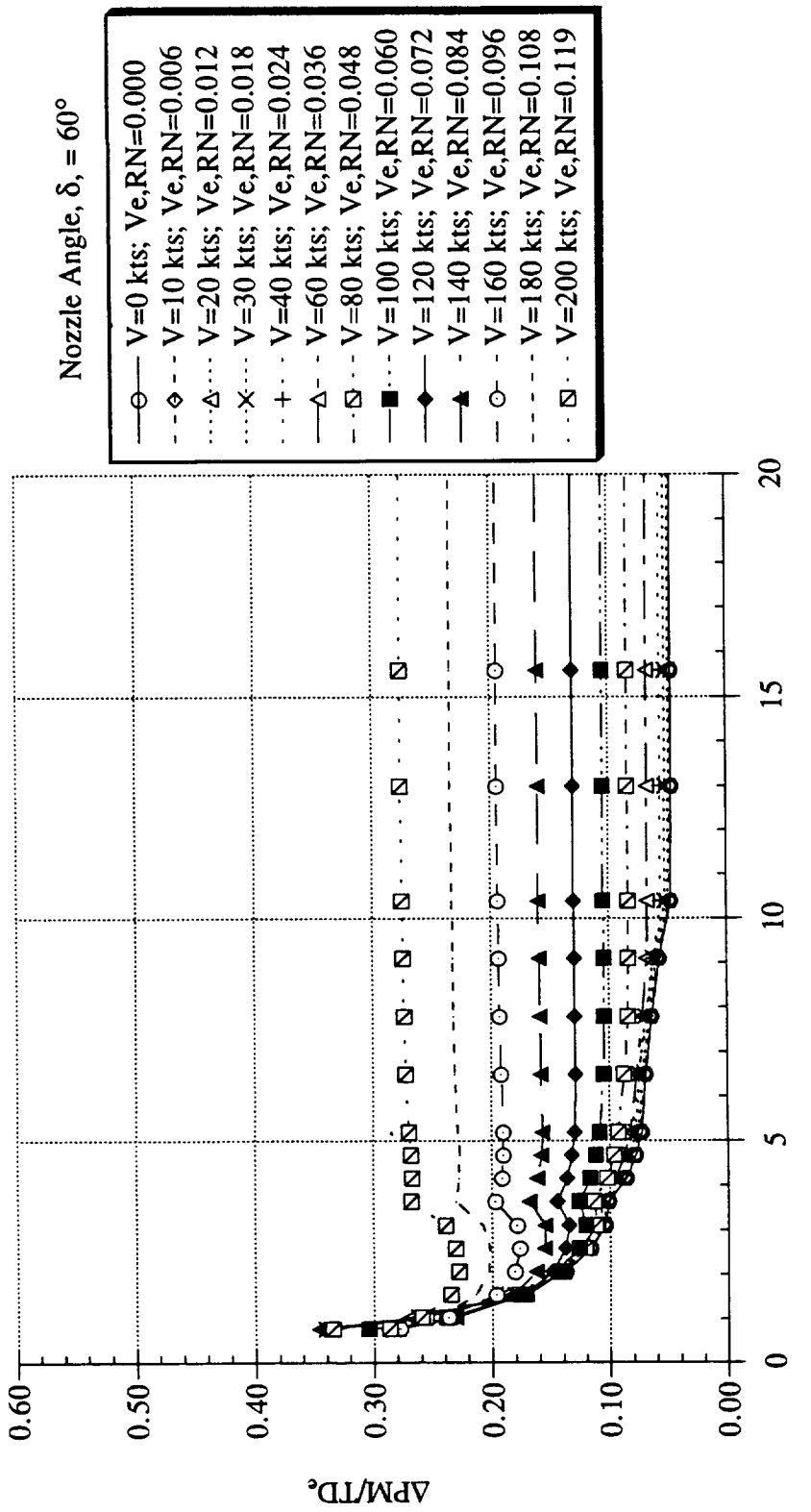

Figure 33. Jet-induced pitching moment increment due to the lift nozzles for various forward velocities, lift nozzles = 60°

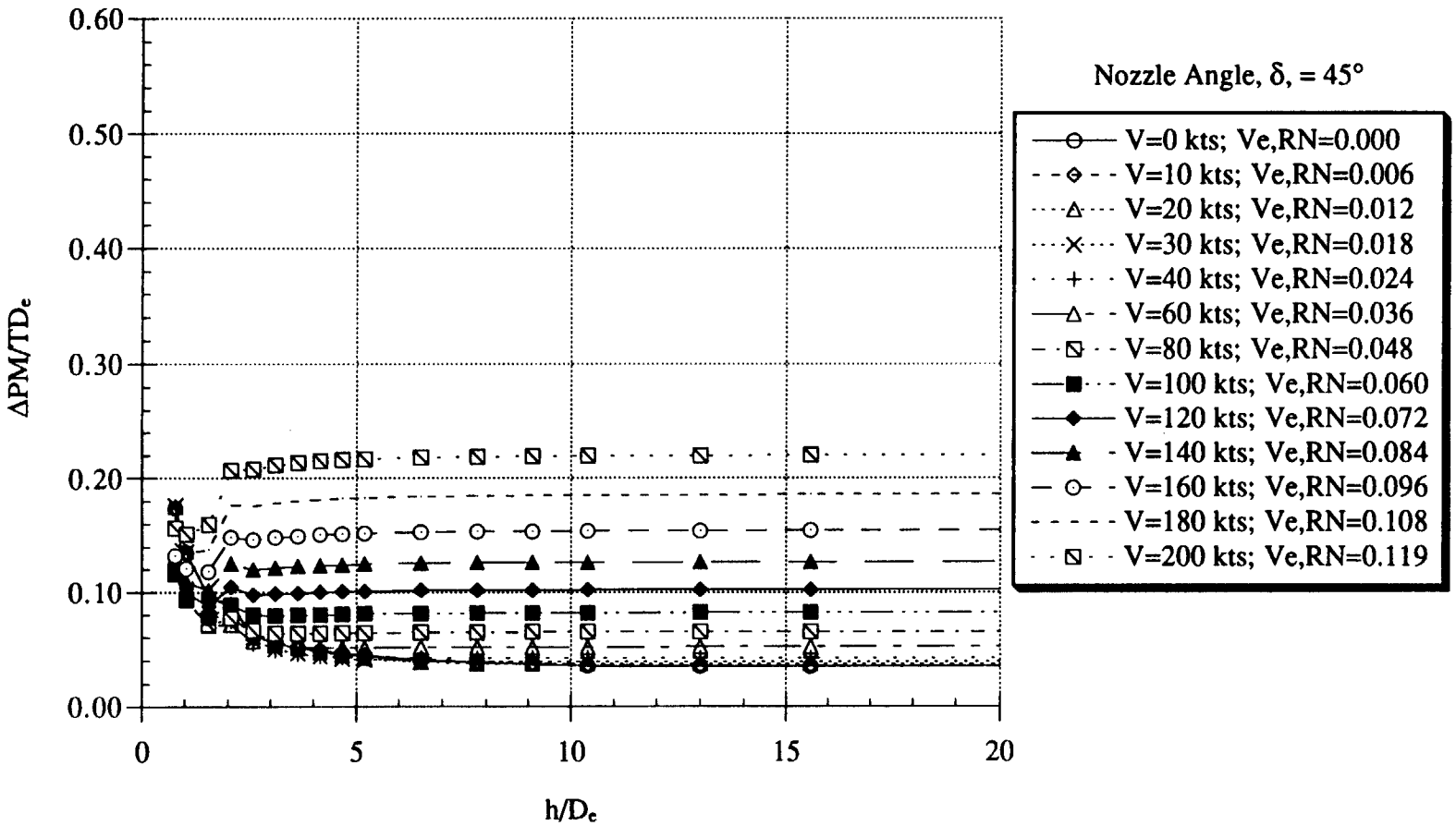

Figure 34. Jet-induced pitching moment increment due to the lift nozzles for various forward velocities, lift nozzles = 45°

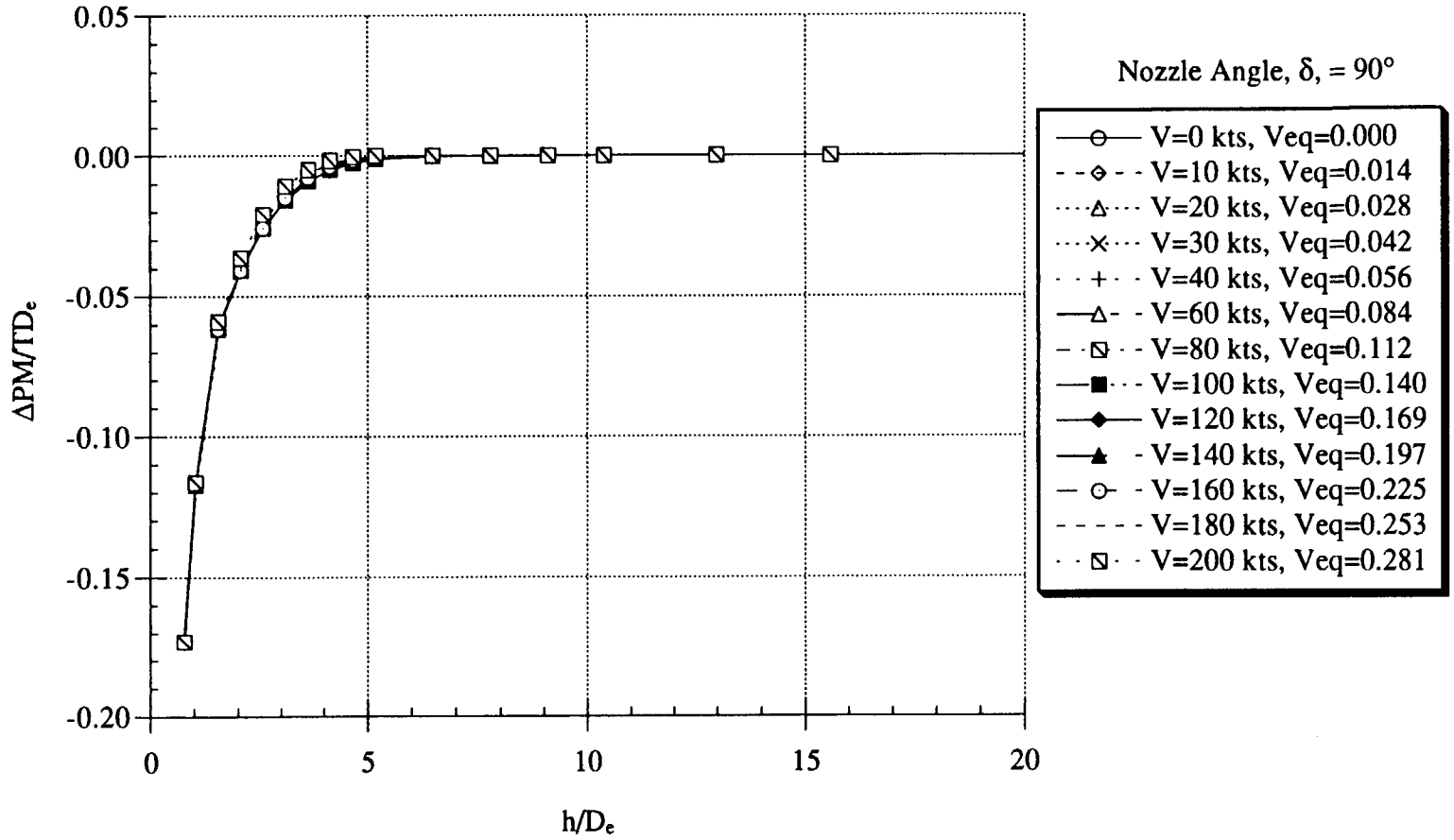

Figure 35. Jet-induced pitching moment increment due to the fountain for various forward velocities, equivalent lift-fan and lift nozzles = 90°

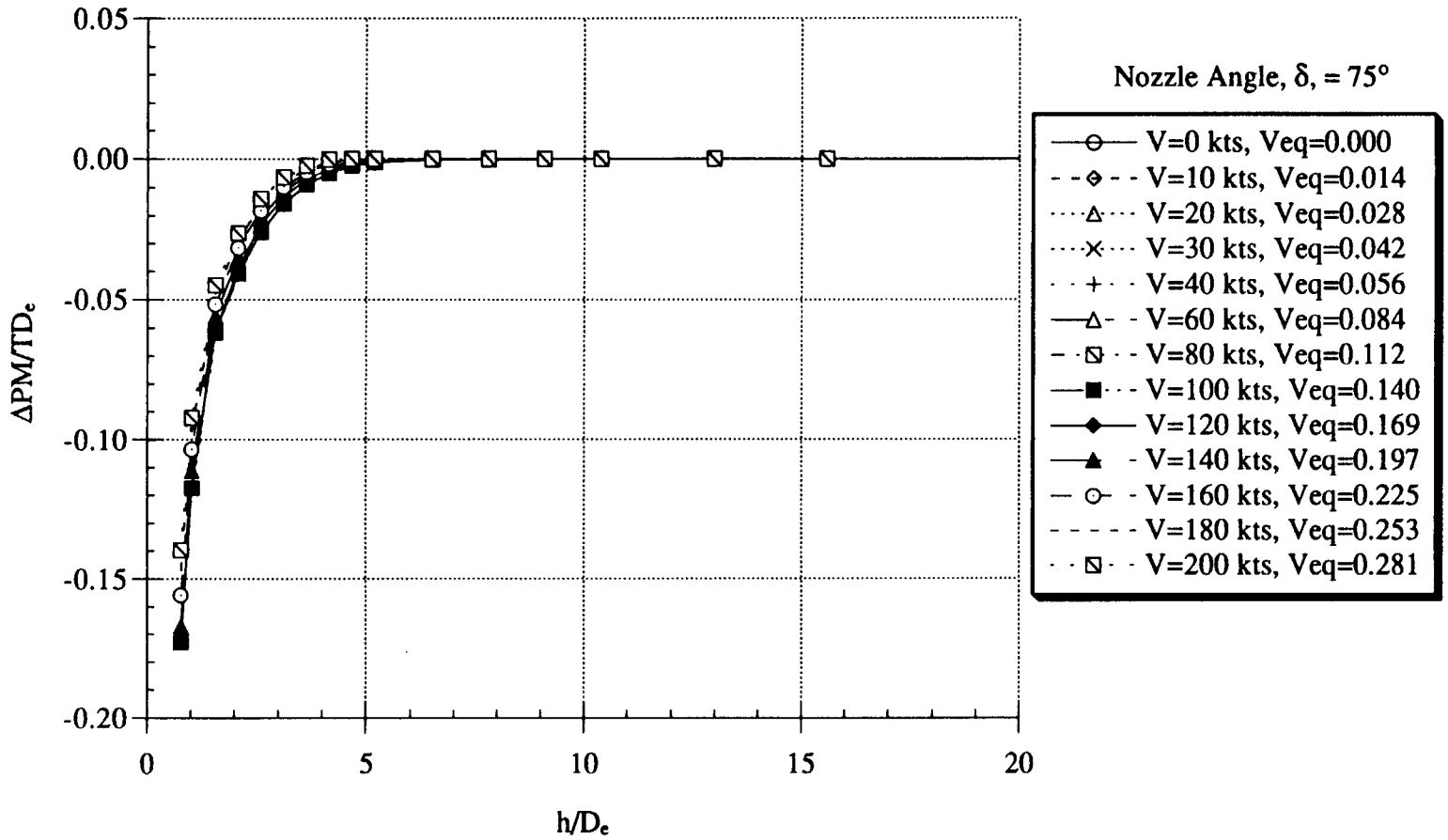

Figure 36. Jet-induced pitching moment increment due to the fountain for various forward velocities, equivalent lift-fan and lift nozzles = 75°

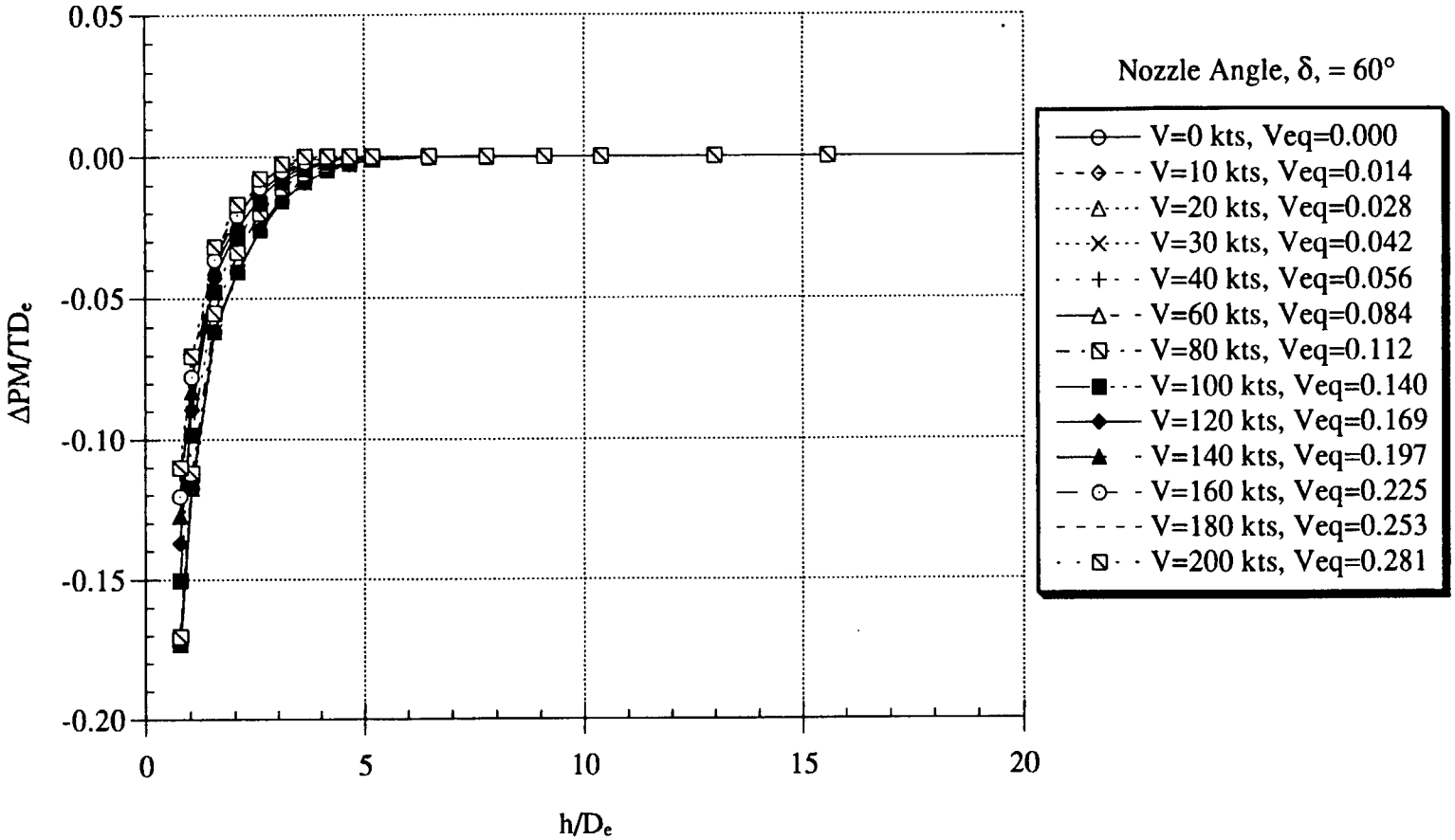

Figure 37. Jet-induced pitching moment increment due to the fountain for various forward velocities, equivalent lift-fan and lift nozzles = 60°

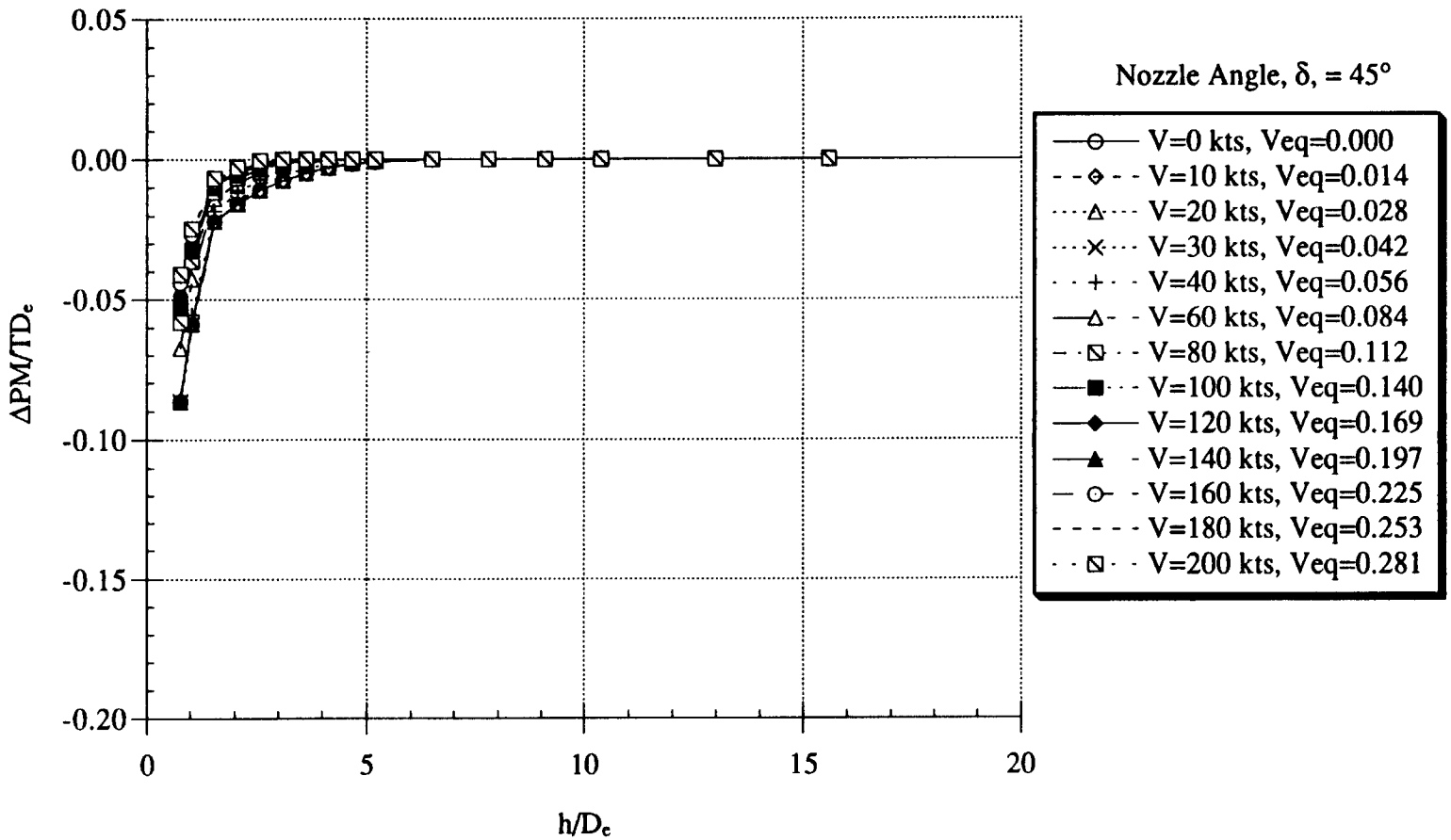

Figure 38. Jet-induced pitching moment increment due to the fountain for various forward velocities, equivalent lift-fan and lift nozzles = 45°

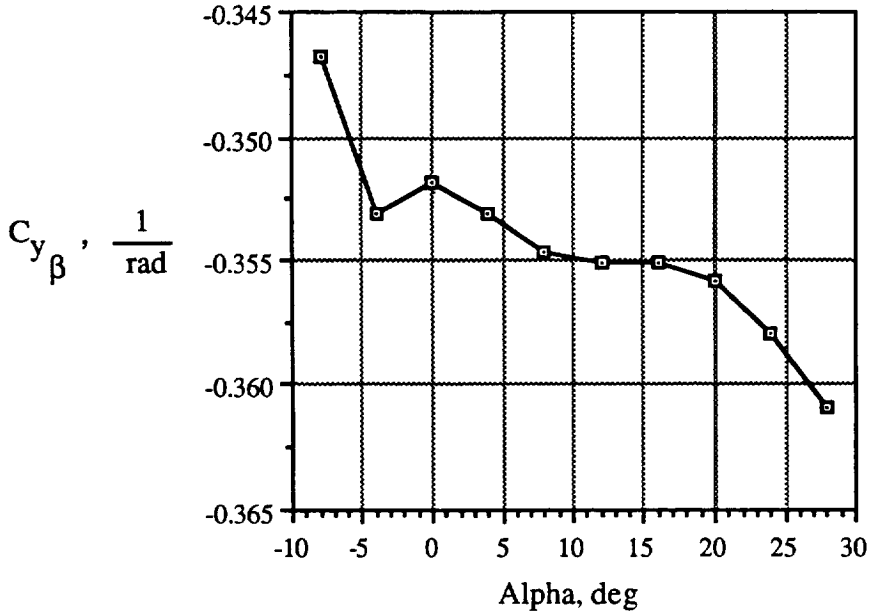

Figure 39. Side force coefficient due to sideslip

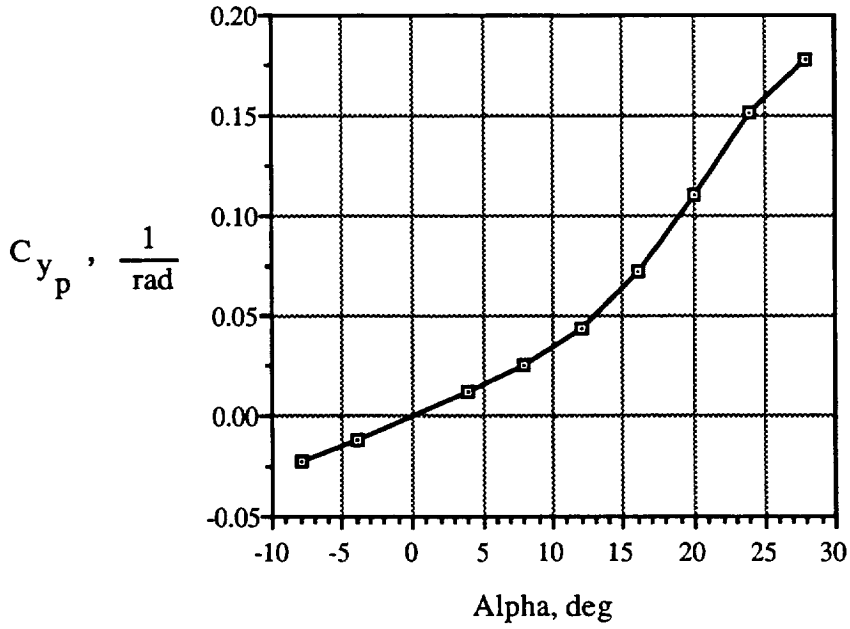

Figure 40. Side force coefficient due to roll rate

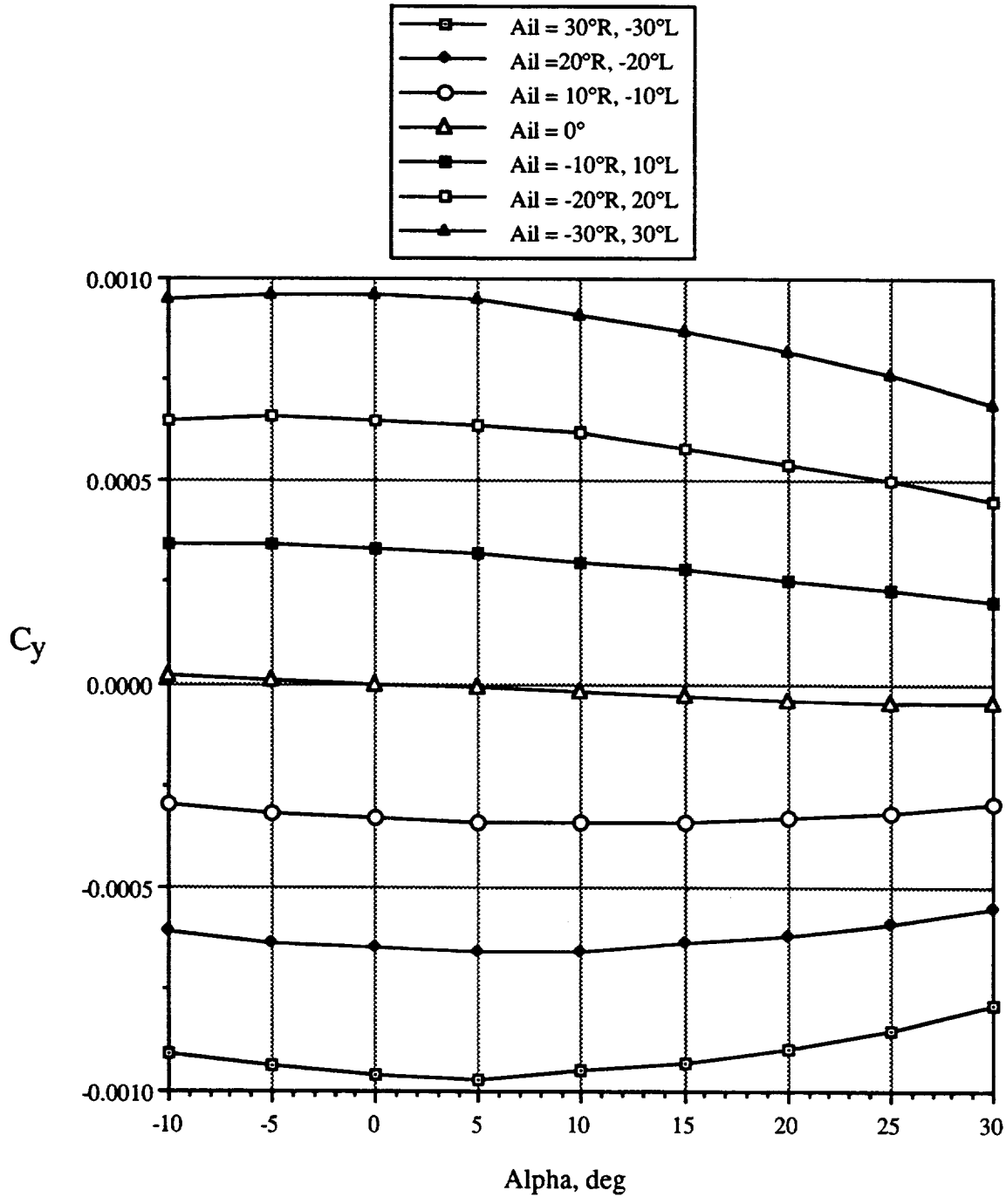

Figure 41. Side force coefficient for various aileron deflections, M = 0.2

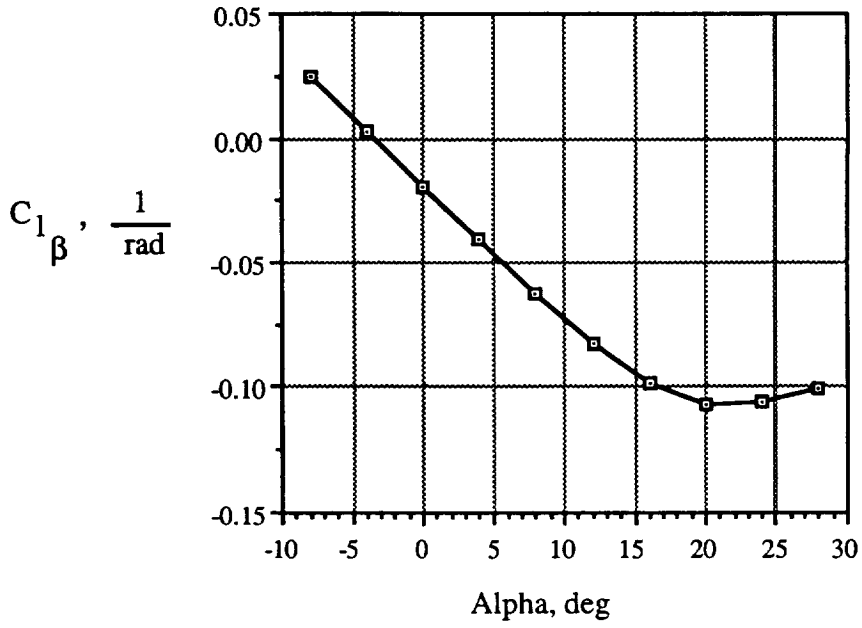

Figure 42. Rolling moment coefficient due to sideslip

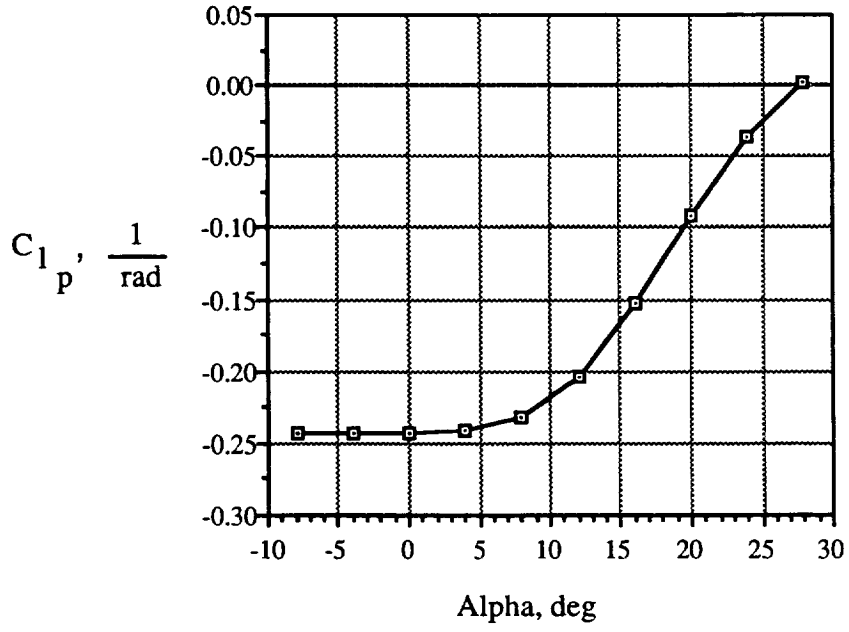

Figure 43. Rolling moment coefficient due to roll rate

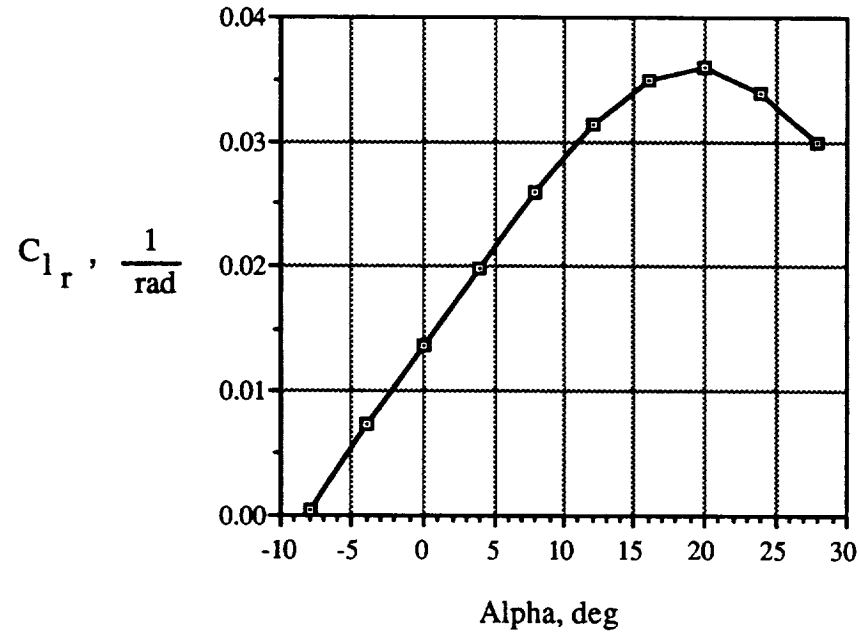

Figure 44. Rolling moment coefficient due to yaw rate

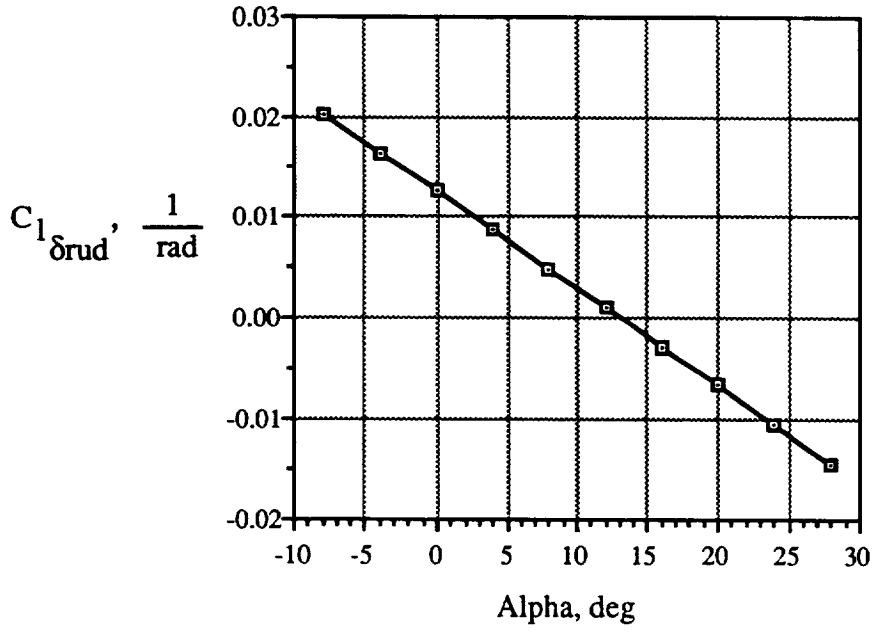

Figure 45. Rolling moment coefficient due to rudder deflection

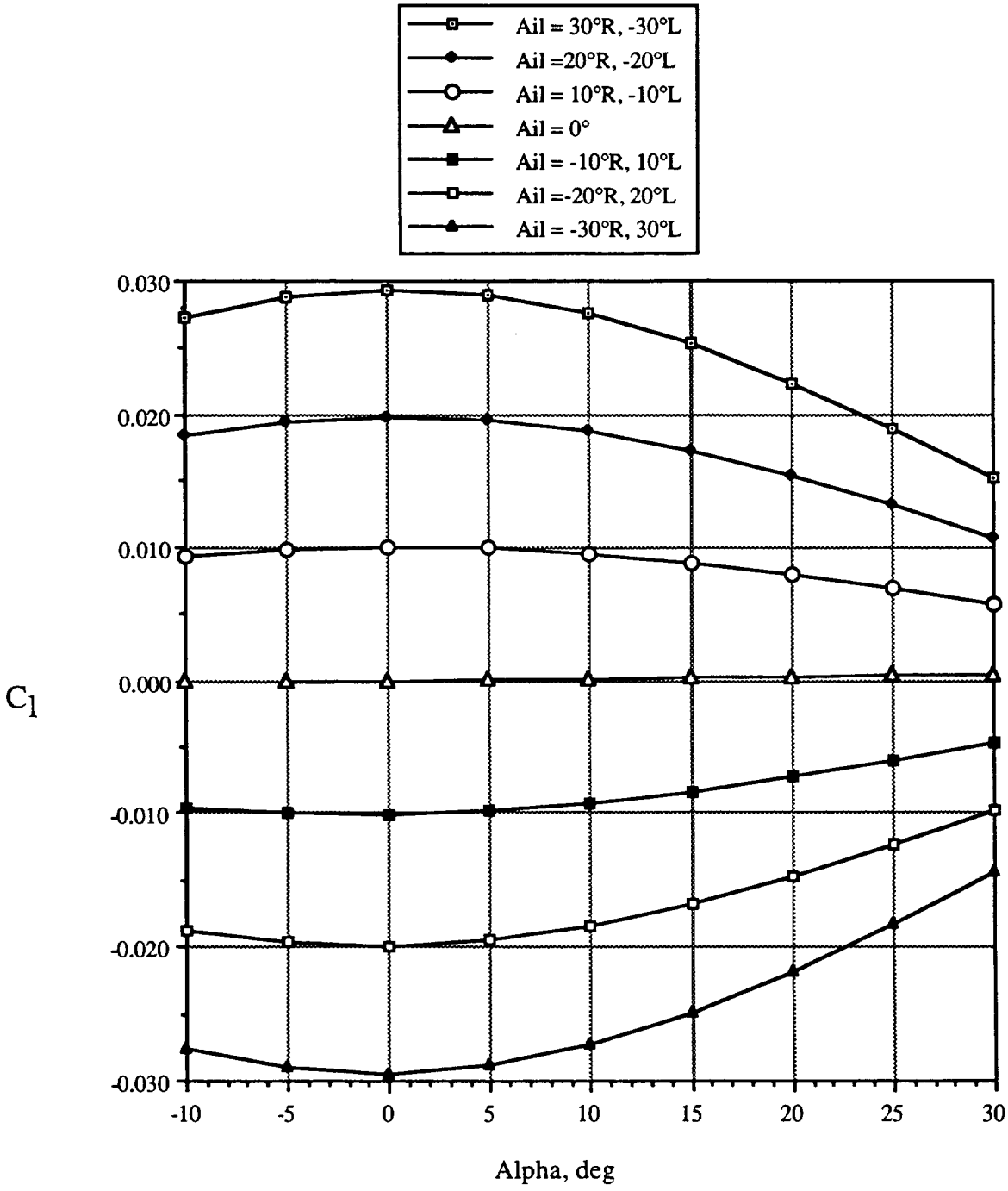

Figure 46. Rolling moment coefficient for various aileron deflections, M = 0.2

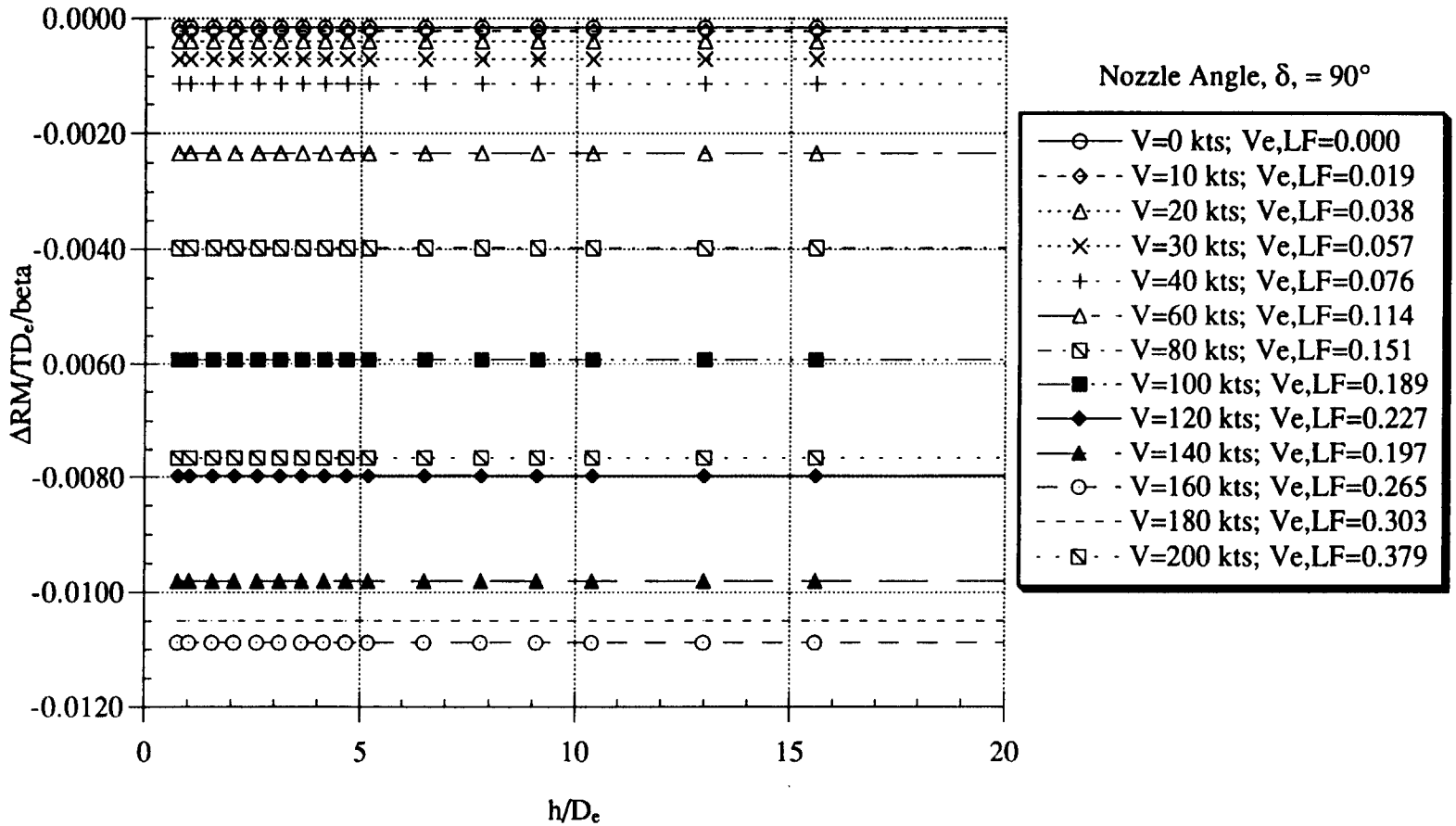

Figure 47. Jet-induced rolling moment increment due to the lift fan for various forward velocities, lift-fan nozzle = 90°

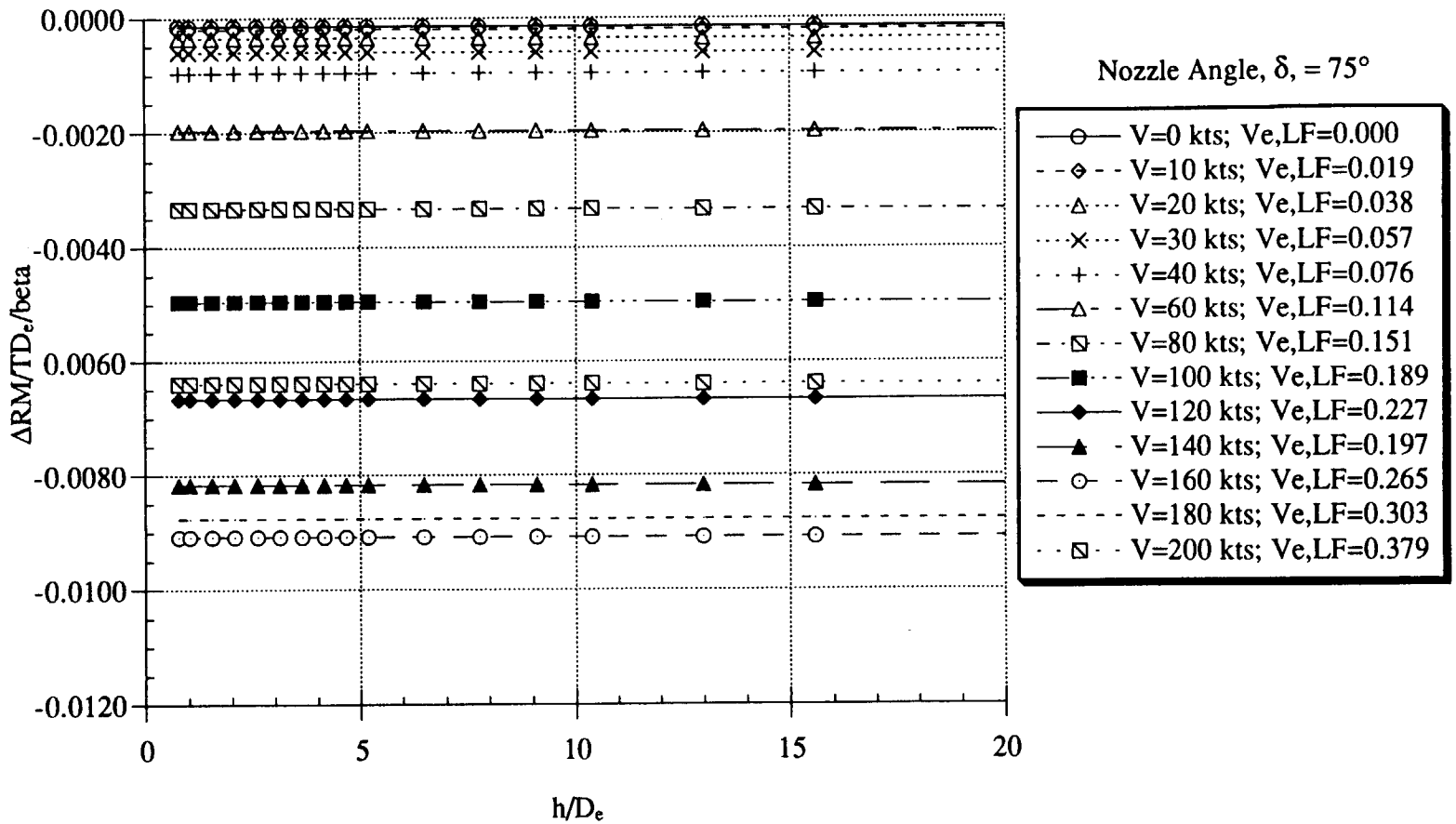

Figure 48. Jet-induced rolling moment increment due to the lift fan for various forward velocities, lift-fan nozzle = 75°

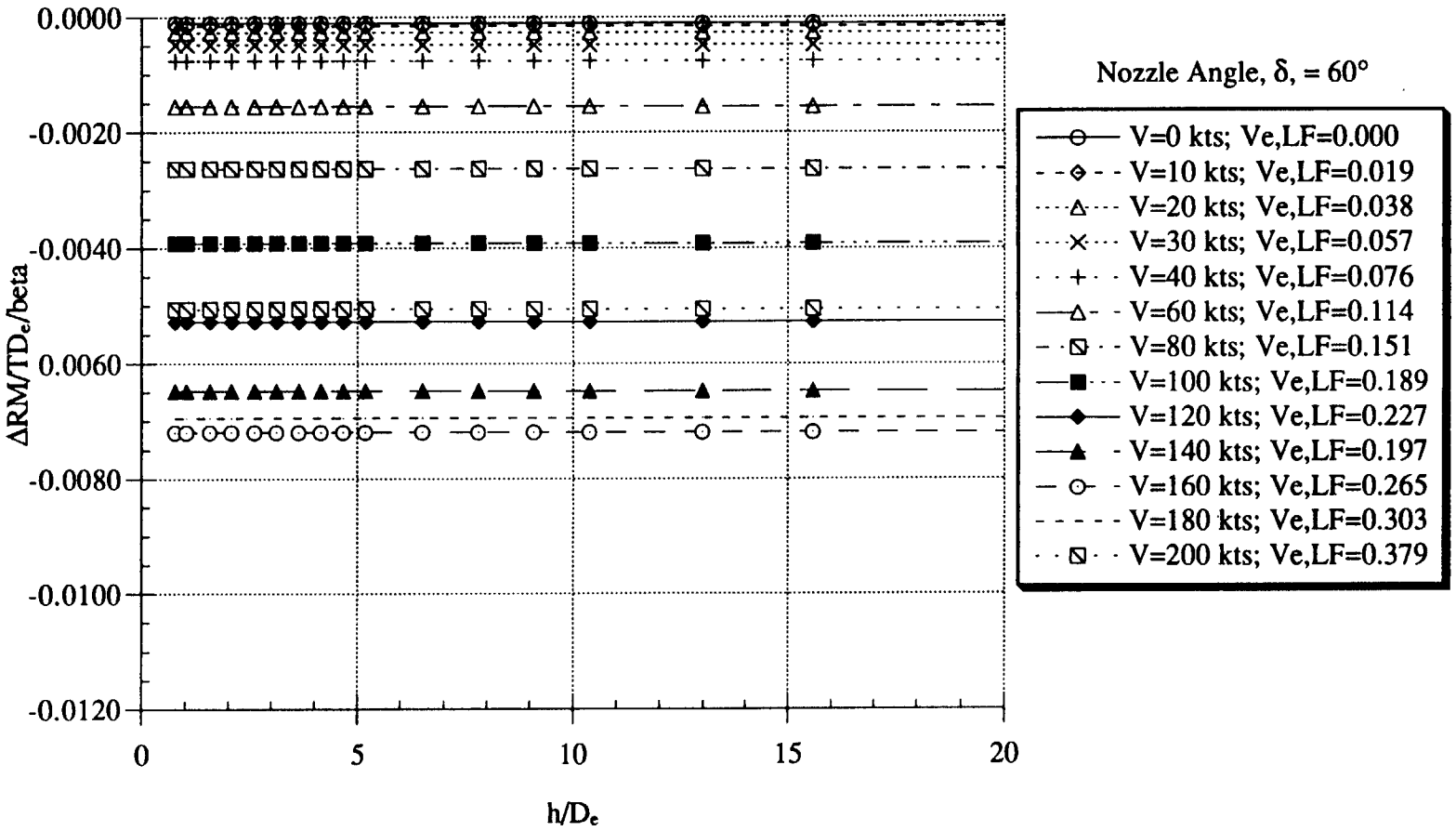

Figure 49. Jet-induced rolling moment increment due to the lift fan for various forward velocities, lift-fan nozzle = 60°

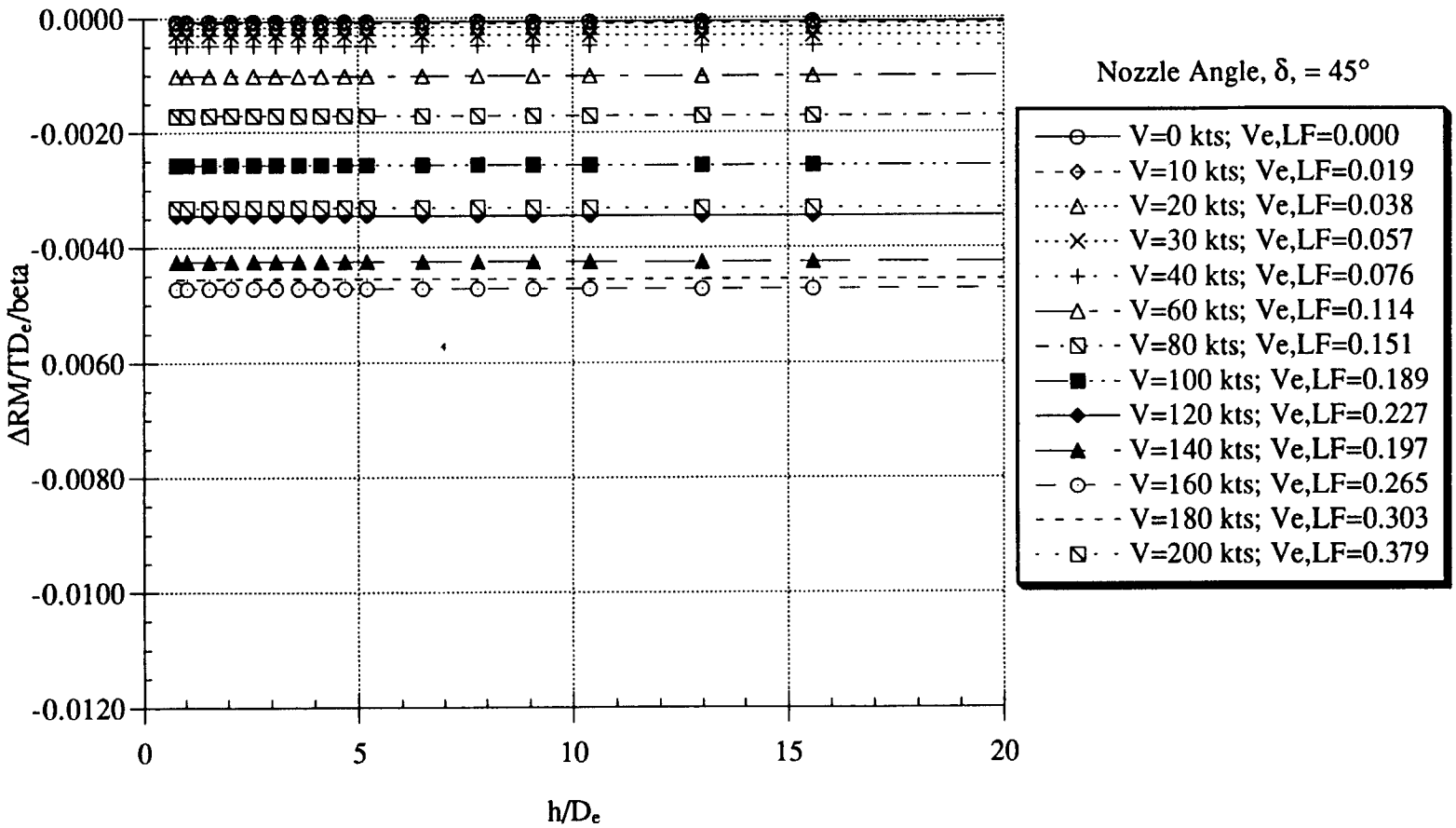

Figure 50. Jet-induced rolling moment increment due to the lift fan for various forward velocities, lift-fan nozzle = 45°

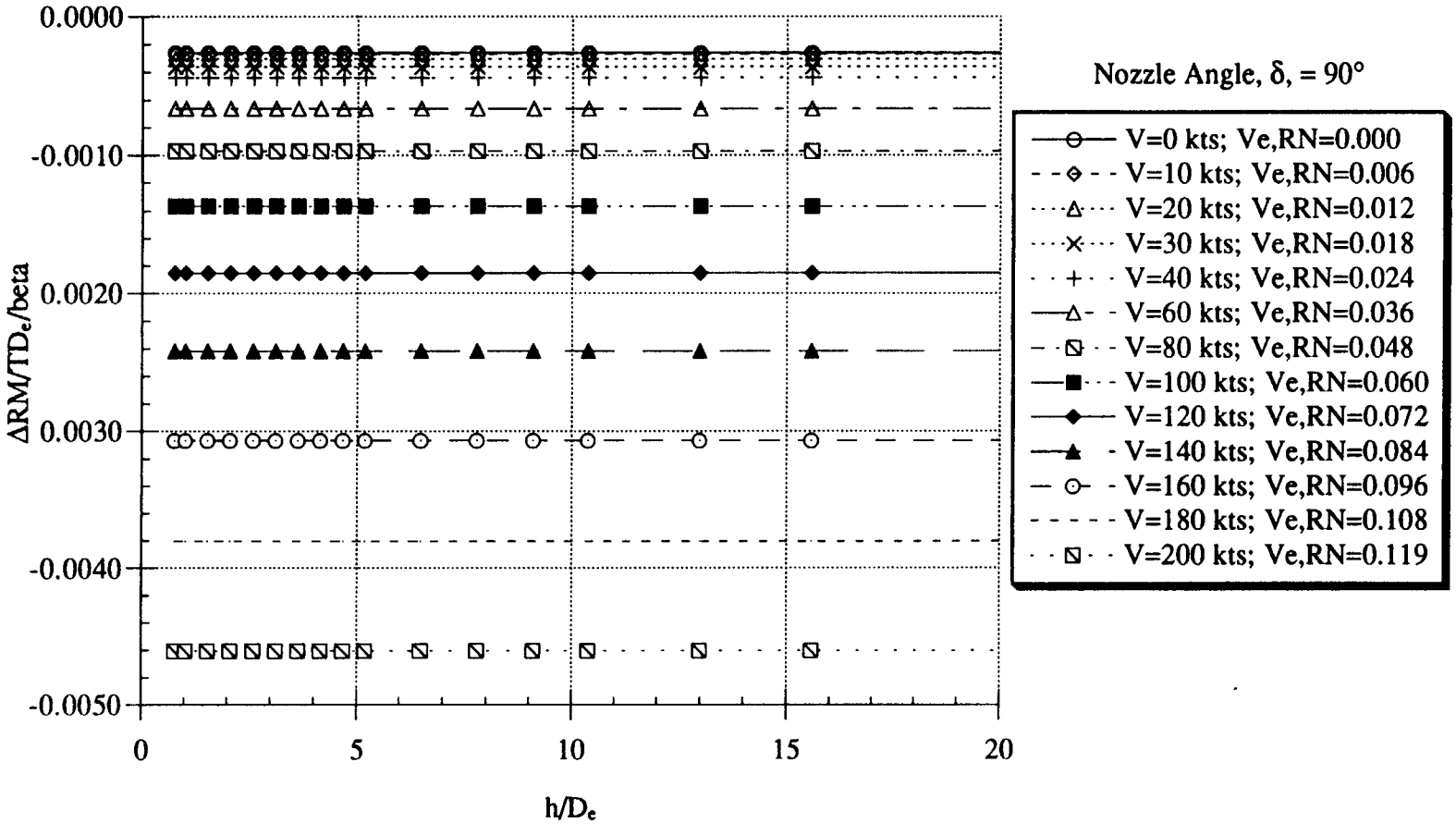

Figure 51. Jet-induced rolling moment increment due to the lift nozzles for various forward velocities, lift nozzles = 90°

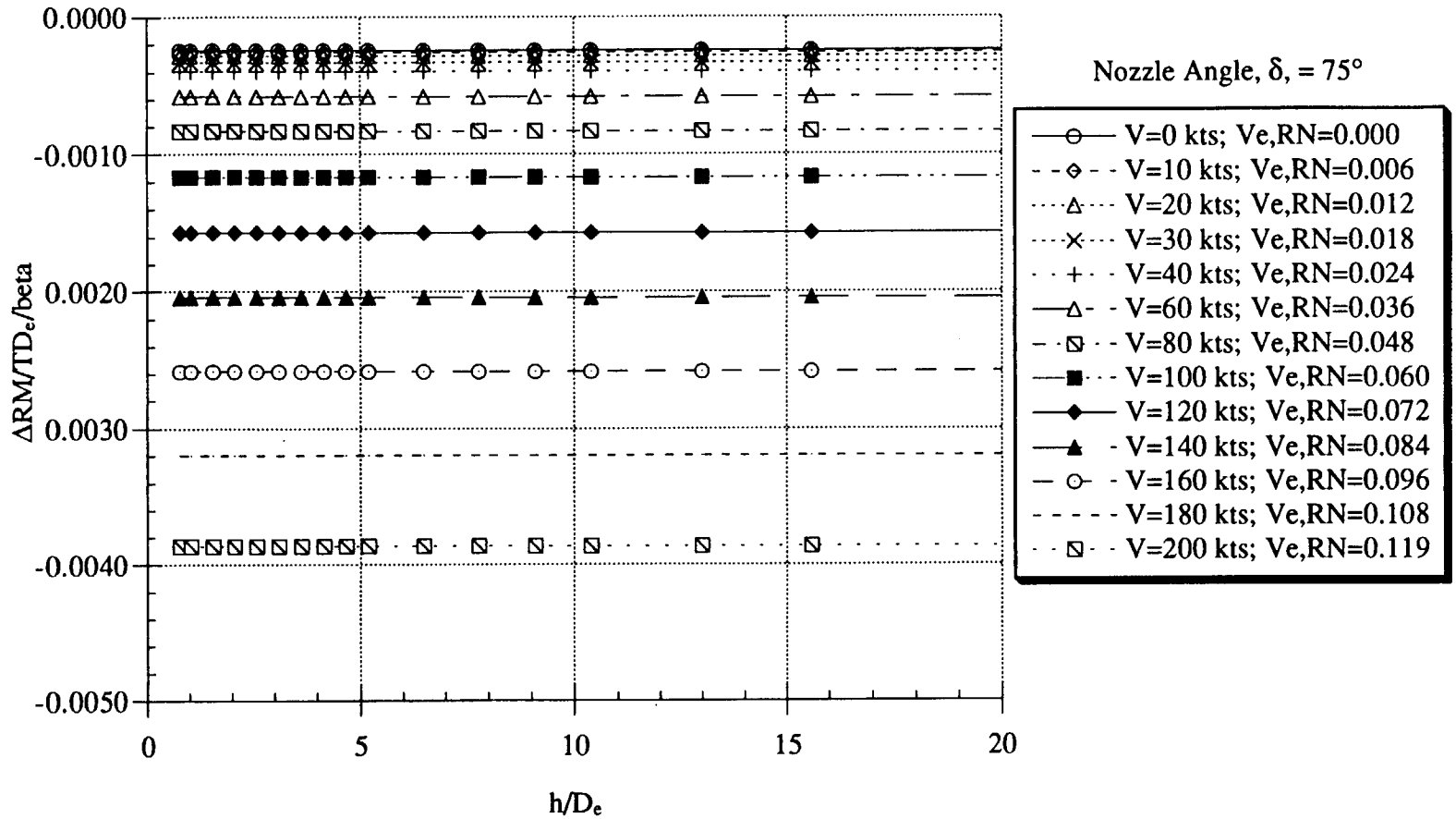

Figure 52. Jet-induced rolling moment increment due to the lift nozzles for various forward velocities, lift nozzles = 75°

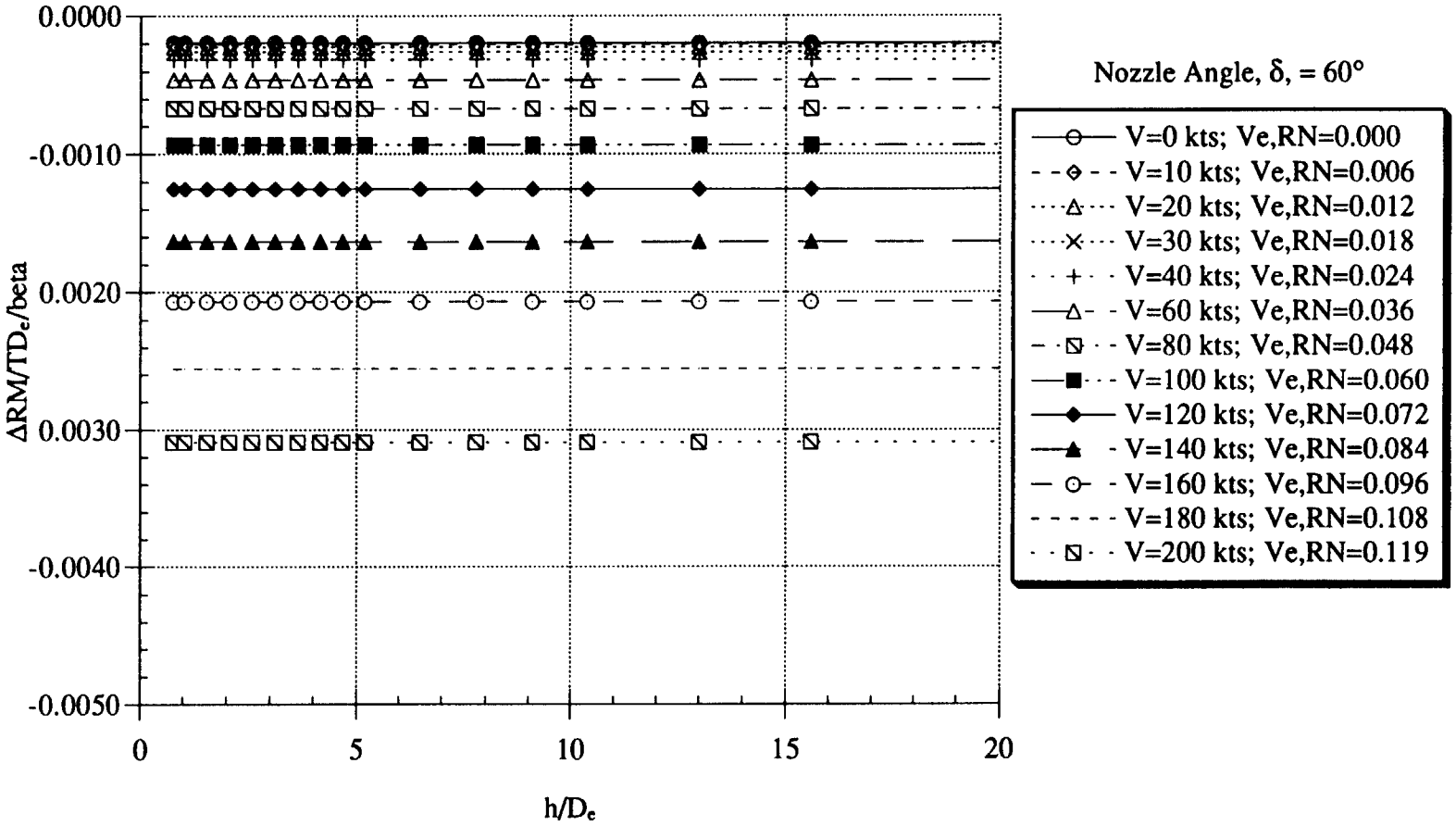

Figure 53. Jet-induced rolling moment increment due to the lift nozzles for various forward velocities, lift nozzles = 60°

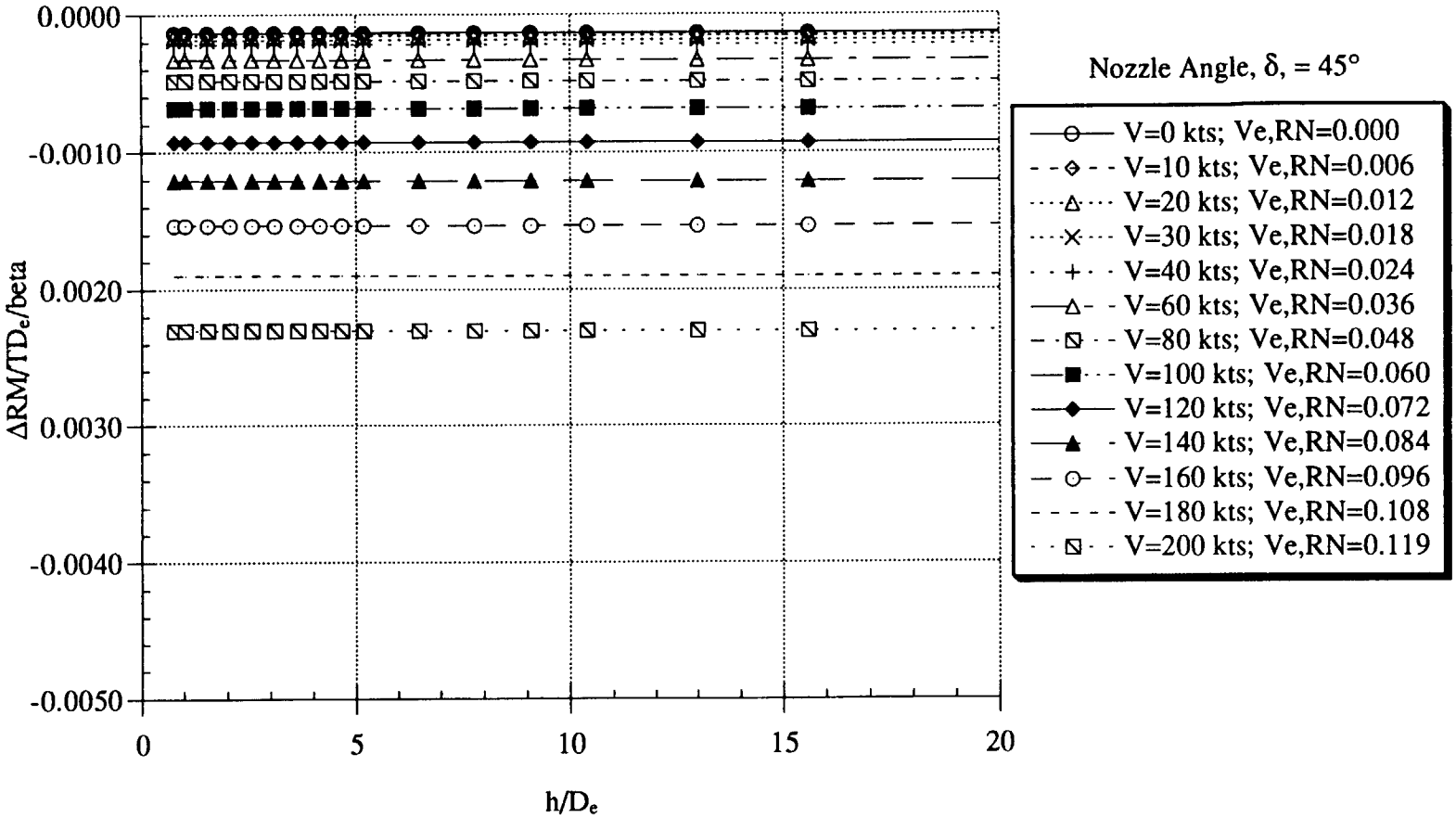

Figure 54. Jet-induced rolling moment increment due to the lift nozzles for various forward velocities, lift nozzles = 45°

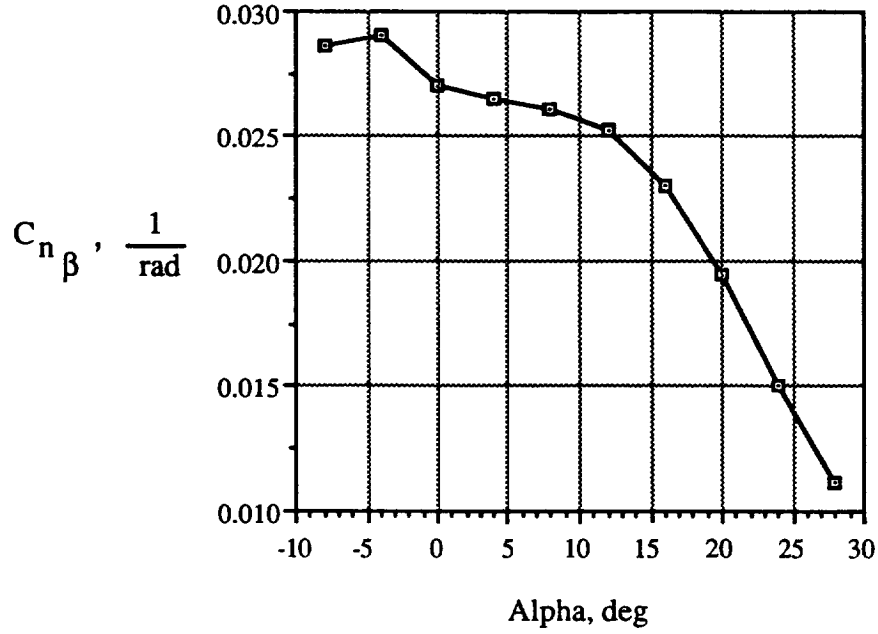

Figure 55. Yawing moment coefficient due to sideslip

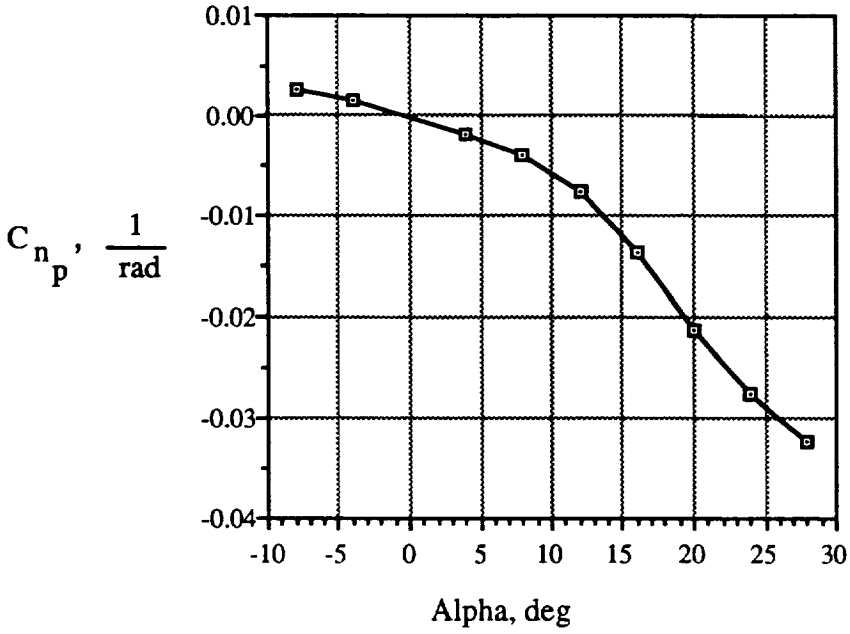

Figure 56. Yawing moment coefficient due to roll rate

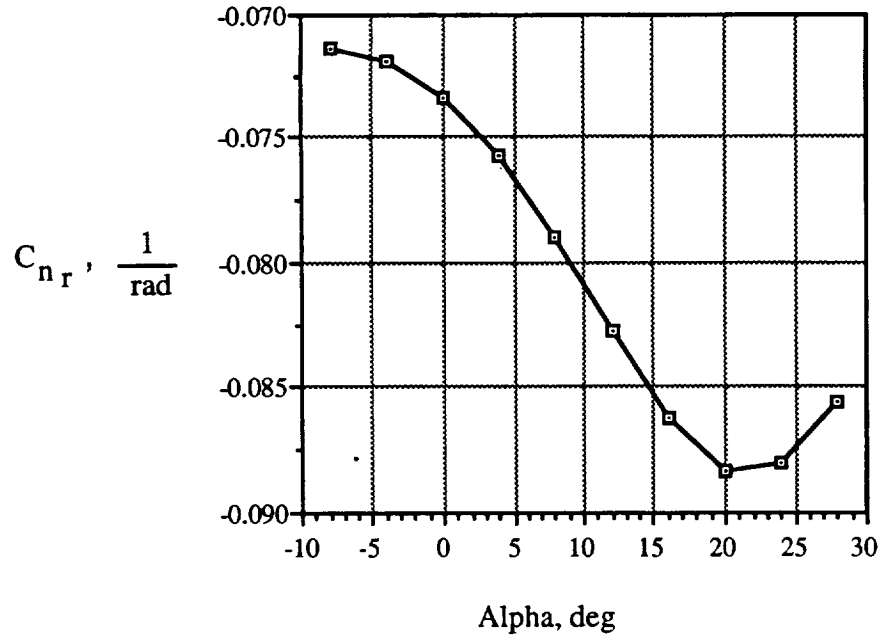

Figure 57. Yawing moment coefficient due to yaw rate

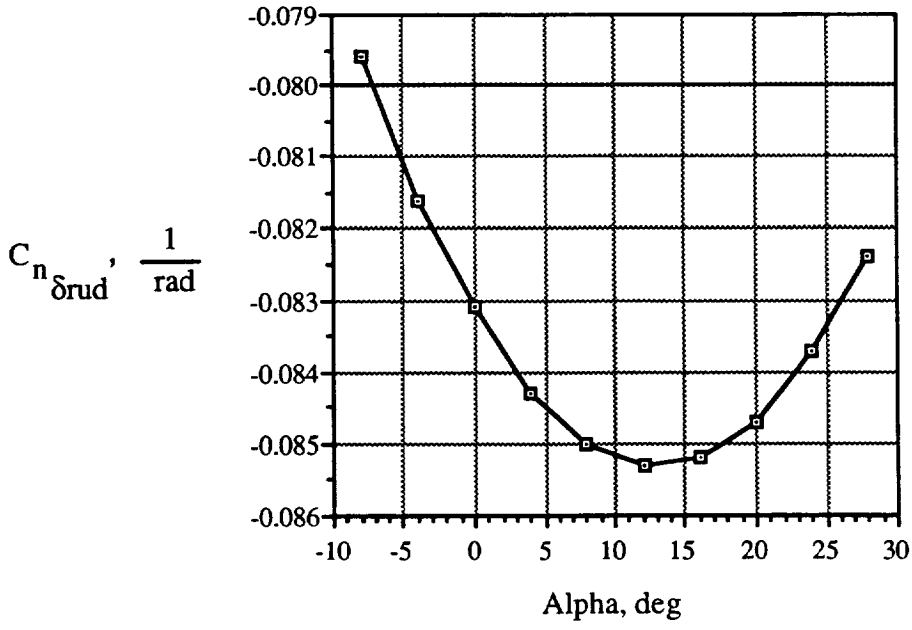

Figure 58. Yawing moment coefficient due to rudder deflection

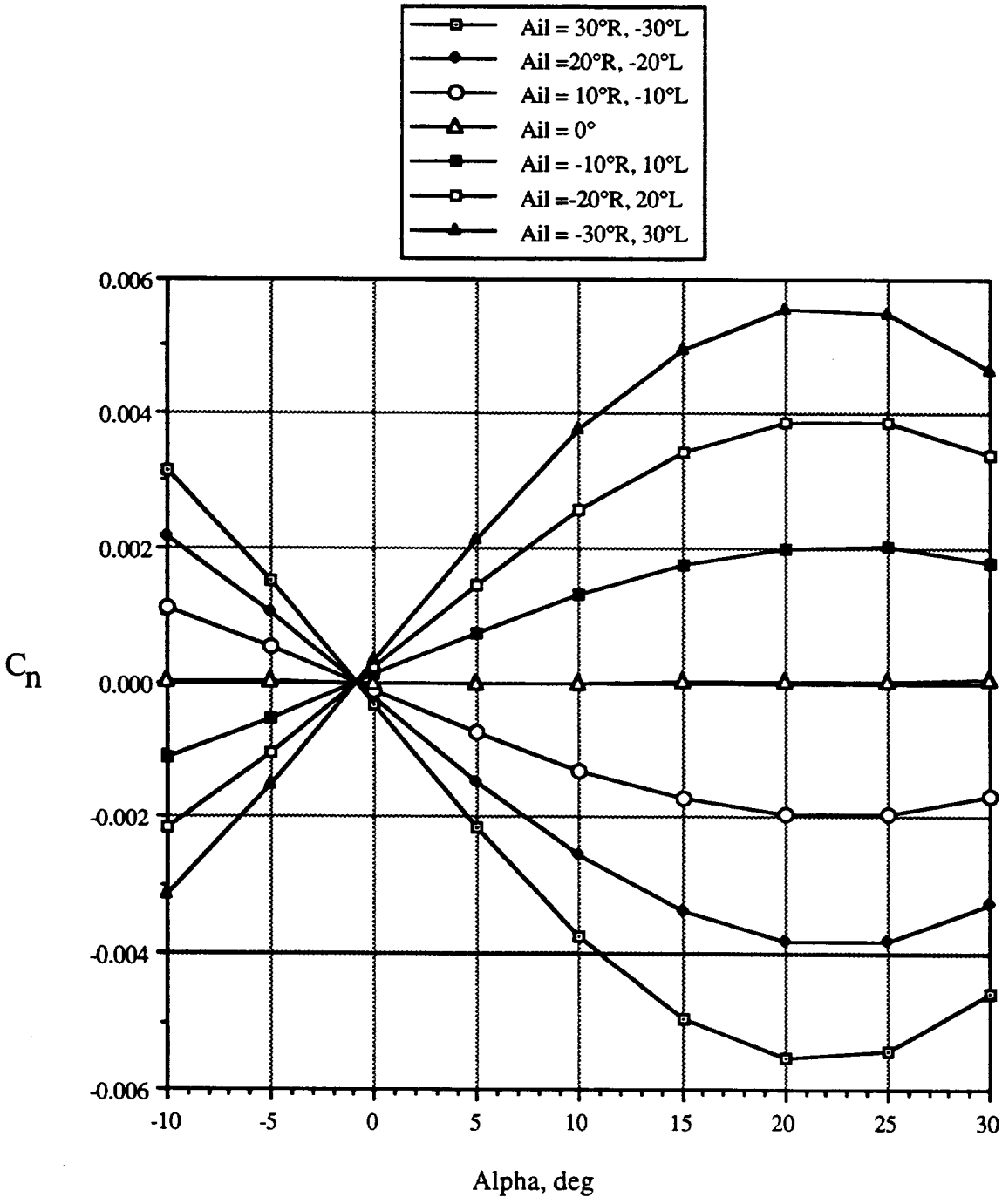

Figure 59. Yawing moment coefficient for various aileron deflections, M = 0.2

REPORT DOCUMENTATION PAGE

Form Approved
OMB No. 0704-0188

1. AGENCY USE ONLY *(Leave blank)*	2. REPORT DATE	3. REPORT TYPE AND DATES COVERED
	April 1995	Technical Memorandum

4. TITLE AND SUBTITLE

Aerodynamics Model for a Generic ASTOVL Lift-Fan Aircraft

5. FUNDING NUMBERS

505-68-32

6. AUTHOR(S)

Lourdes G. Birckelbaw, Walter E. McNeill, and Douglas A. Wardwell

7. PERFORMING ORGANIZATION NAME(S) AND ADDRESS(ES)

Ames Research Center
Moffett Field, CA 94035-1000

8. PERFORMING ORGANIZATION REPORT NUMBER

A-950051

9. SPONSORING/MONITORING AGENCY NAME(S) AND ADDRESS(ES)

National Aeronautics and Space Administration
Washington, DC 20546-0001

10. SPONSORING/MONITORING AGENCY REPORT NUMBER

NASA TM-110347

11. SUPPLEMENTARY NOTES

Point of Contact: Lourdes G. Birckelbaw, Ames Research Center, MS 237-2, Moffett Field, CA 94035-1000
(415) 604-5592

12a. DISTRIBUTION/AVAILABILITY STATEMENT

Unclassified — Unlimited
Subject Category 02

12b. DISTRIBUTION CODE

13. ABSTRACT ***(Maximum 200 words)***

This report describes the aerodynamics model used in a simulation model of an advanced short takeoff and vertical landing lift-fan fighter aircraft. The simulation model was developed for use in piloted evaluations of transition and hover flight regimes, so that only low speed (M ~ 0.2) aerodynamics are included in the mathematical model. The aerodynamic model includes the power-off aerodynamic forces and moments and the propulsion system induced aerodynamic effects, including ground effects.

The power-off aerodynamics data were generated using the U.S. Air Force Stability and Control Digital DATCOM program and a NASA Ames in-house graphics program called VORVIEW which allows the user to easily analyze arbitrary conceptual aircraft configurations using the VORLAX program. The jet-induced data were generated using the prediction methods of R. E. Kuhn et al., as referenced in this report.

14. SUBJECT TERMS

ASTOVL, Lift fan, Aerodynamics model

15. NUMBER OF PAGES

63

16. PRICE CODE

A04

17. SECURITY CLASSIFICATION OF REPORT	18. SECURITY CLASSIFICATION OF THIS PAGE	19. SECURITY CLASSIFICATION OF ABSTRACT	20. LIMITATION OF ABSTRACT
Unclassified	Unclassified		